

Joint cardiac tissue conductivity and activation time estimation using confirmatory factor analysis

Sun, Miao; de Groot, Natasja M.S.; Hendriks, Richard C.

DOI

[10.1016/j.compbimed.2022.105393](https://doi.org/10.1016/j.compbimed.2022.105393)

Publication date

2022

Document Version

Final published version

Published in

Computers in Biology and Medicine

Citation (APA)

Sun, M., de Groot, N. M. S., & Hendriks, R. C. (2022). Joint cardiac tissue conductivity and activation time estimation using confirmatory factor analysis. *Computers in Biology and Medicine*, 144, Article 105393. <https://doi.org/10.1016/j.compbimed.2022.105393>

Important note

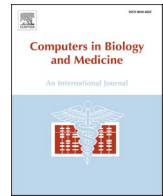
To cite this publication, please use the final published version (if applicable).
Please check the document version above.

Copyright

Other than for strictly personal use, it is not permitted to download, forward or distribute the text or part of it, without the consent of the author(s) and/or copyright holder(s), unless the work is under an open content license such as Creative Commons.

Takedown policy

Please contact us and provide details if you believe this document breaches copyrights.
We will remove access to the work immediately and investigate your claim.



Joint cardiac tissue conductivity and activation time estimation using confirmatory factor analysis

Miao Sun^{a,*}, Natasja M.S. de Groot^b, Richard C. Hendriks^a

^a Faculty of Electrical Engineering, Mathematics and Computer Science, Delft University of Technology, the Netherlands

^b Department of Cardiology, Erasmus University Medical Center, the Netherlands

ARTICLE INFO

Keywords:

Conductivity estimation
Activation time estimation
Cross power spectral density
Confirmatory factor analysis

ABSTRACT

Mathematical models of the electrophysiology of cardiac tissue play an important role when studying heart rhythm disorders like atrial fibrillation. Model parameters such as conductivity, activation time, and anisotropy ratio are useful parameters to determine the arrhythmogenic substrate that causes abnormalities in the atrial tissue. Existing methods often estimate the model parameters separately and assume some of the parameters to be known as a priori knowledge. In this work, we propose an efficient method to jointly estimate the parameters of interest from the cross power spectral density matrix (CPSDM) model of the electrograms. By applying confirmatory factor analysis (CFA) to the CPSDMs of multi-electrode electrograms, we can make use of the spatial information of the data and analyze the relationship between the desired resolution and the required amount of data. With the reasonable assumptions that the conductivity parameters and the anisotropy parameters are constant across different frequencies and heart beats, we estimate these parameters using multiple frequencies and multiple heart beats simultaneously to easier satisfy the identifiability conditions in the CFA problem. Results on the simulated data show that using multiple heart beats decreases the estimation errors of the conductivity and the estimated activation time parameters. The experimental results on clinical data show that using multiple heart beats for parameter estimation can reduce the reconstruction errors of the clinical electrograms, which further demonstrates the robustness of the proposed method.

1. Introduction

Mathematical modeling of the electrophysiological properties of atrial tissue could play an important role in understanding atrial fibrillation and detecting the underlying arrhythmogenic substrate. Previous research has been shown that development and progression of cardiac arrhythmias are related to impaired conduction in cardiac tissue [1–5]. As such, these models should, among other things, include cell and tissue properties like the cell conductivity, the anisotropy ratio of the conductivity and the cell's activation time to accurately describe the propagation of the electrical waves. Such models have been proposed in previous research, e.g., [6–9]. In addition to the (forward) modelling itself, being able to accurately determine these model parameters from measurements is at least as important to be able to investigate the cause of cardiac arrhythmias and localize the arrhythmogenic substrate in the tissue. However, such inversion problems are often rather challenging due to the limited amount of measurements on one hand, and the large number of desired parameters on the other hand. The study in [9]

estimated the tissue conductivities from the transmembrane action potential of each cell that were directly obtained using micro-electrode arrays. However, this is impractical for living human tissue. More recently, Abdi. et al. [10] proposed a simplified forward model to replace the computationally intensive reaction-diffusion equations for describing the electrical propagation in atrial tissue, which reduces the computation cost of calculating all cell action potentials. They assumed that an electrogram is a summation of electrical activity of cell groups surrounding the electrode location and proposed a deconvolution method to estimate the tissue conductivities. However, this approach did not make use of spatial information of multi-electrode data and assumed the anisotropy ratio and the activation time of the cells are known. Finally, the activation time was estimated using the steepest descent method before estimating conductivity parameters. Cardiologists often use the less complex conduction velocity to analyze the electrical propagation and electropathology [1,11]. However, conduction velocity is not very reliable for investigating the arrhythmogenic substrates in cardiac tissue, since the conduction velocity can be

* Corresponding author.

E-mail address: M.Sun@tudelft.nl (M. Sun).

<https://doi.org/10.1016/j.combiomed.2022.105393>

Received 15 October 2021; Received in revised form 7 March 2022; Accepted 8 March 2022

Available online 11 March 2022

0010-4825/© 2022 The Authors. Published by Elsevier Ltd. This is an open access article under the CC BY license (<http://creativecommons.org/licenses/by/4.0/>).

changed by both pathological origins or non-pathological origins like local curvature [2].

We have recently proposed the use of an efficient method called confirmatory factor analysis (CFA) to jointly estimate a subset of the useful parameters, that are the tissue conductivity and the anisotropy ratio from electrograms [12]. By analyzing the identifiability conditions in the formulated CFA problem, we find the relation between the required amount of data and the desired resolution. However, the method presented in [12] was limited to the use of a single heart beat and could only estimate the conductivity and the anisotropy parameters. In this work, we further extend this algorithm to jointly estimate the conductivity, anisotropy ratio, as well as the activation time per cell using multiple heart beats and multiple frequencies by using the proposed method called simultaneous CFA.

CFA is a type of modeling that can deal with the relationships between observed measures and latent variables [13]. In CFA, a factor is a variable that influences more than one observed measure and affects the correlations among the observed measures. The goal of a factor analysis model is to establish the number and nature of factors that account for the variation and covariation among the observed measures. Therefore, CFA has been widely used to test whether the data fits a hypothesized measurement model that captures the variance-covariance structures of the measurements [13]. To estimate the parameters in the CFA model and reproduce the variance-covariance matrix, constraints are often imposed on the model. These are based on a priori knowledge that is required to satisfy the identifiability conditions in the CFA problem [14–17]. In our previous work [12], we have applied CFA to the cross-power spectral density (CPSDM) model of the measurements to estimate the conductivity parameters and the anisotropy ratio parameters. In order to easier satisfy the identifiability conditions, we assumed that the conductivity parameters and the anisotropy ratio parameters are roughly constant across frequencies within a certain range and proposed simultaneous CFA (SCFA) using multiple temporal frequencies of a single heart beat. Although [18] showed that in general conductivity is frequency dependent for the human heart, it follows from [18] that the conductivity is nearly constant within the frequency range from 0 to 100 Hz that we considered. The activation time parameters were assumed to be known and were in the end estimated by the steepest descent method, as described in [19], before estimating the conductivity.

In this work, we propose a more efficient SCFA method to jointly estimate more model parameters from epicardial electrograms. It is based on the fact that the propagation of the electrical wave in the tissue might change its direction slightly from one heart beat to another, even during sinus rhythm (SR). Multiple of these heart beats then “illuminate” the tissue from (slightly) different directions and provide additional and different data that could facilitate the parameter estimation. Taking this into account, we further make use of multiple heartbeats to improve the parameter estimation. Since the conductivity and the anisotropy ratio parameters are roughly constant in different frequencies and different heart beats, we estimate these parameters across multiple frequencies and heart beats to increase the ratio between the number of equations and the number of unknown parameters in the SCFA problem. However, note that the activation time parameters will change across different heart beats and are therefore estimated for each heart beat. In order to utilize the spatial structure of the multi-electrode data, the proposed algorithm is based on the CPSDM model. Extra constraints that incorporate prior knowledge on the model parameters are used to reduce the feasibility set of the parameter space and therefore increase the robustness of the algorithm.

Altogether, this paper makes more efficient use of the data than [12] and further improves the CFA approach for jointly estimating cardiac tissue parameters. More concretely, the differences between this paper and our previous work are as follows: 1) Our previous work was limited to only estimate the conductivity parameters assuming the activation time per cell is known exactly. In this paper we considered to not only

estimate the conductivity and the anisotropy ratio parameters, but also to jointly estimate the activation time parameter; 2) In our previous work, we used only a single heart beat for parameter estimation. This is rather limited as the waveform can come from varying directions in consecutive heart beats. In this paper we therefore used multiple heart beats for estimation. This allows to exploit the fact that the tissue is “illuminated” from different directions, leading to a much better use of the data. Alternatively, one might consider to first obtain parameter estimates per heart beat and then calculate the average, which is not efficient and not effective. In this paper, instead we first analyzed which parameters are constant across heart beats. For the parameters that are constant across heart beats, i.e., the conductivity and the anisotropy ratio parameters, we considered to obtain one estimate of the parameters from multiple heart beats; for the parameters that vary from beat-to-beat, i.e., the activation time parameter, we consider to obtain one estimate per heart beat. In this way we increased the ratio of known to unknown parameters such that a higher spatial resolution of parameters can be obtained given the same amount of data. By updating the values of the activation time with the other two parameters in the same optimization loop, we further improve the estimation accuracy of these parameters.

The rest of the paper is organized as follows. In Section II, we introduce the notation, the impulse response model, the CPSDM model, and the problem formulation for the joint model parameter estimation. In Section III, we review the basic CFA theory and introduce the proposed SCFA algorithm and practical consideration to increase the robustness of the proposed algorithm. In Section IV and V, we evaluate the proposed algorithm using simulated data and clinical data, respectively. In Section VI, we discuss the advantages and the limitations of this work and draw the conclusions.

2. Preliminaries

In this section, we introduce the notation that we use and review the epicardial electrogram models in the time domain and the frequency domain, respectively. Although the details on the time and frequency domain models have been presented in [12], we summarize here the most important aspects to guide the reader.

2.1. Notation

Lower-case letters, bold-face lower-case letters and bold face upper-case letters are used to denote scalars, vectors, and matrices, respectively. For example, a matrix \mathbf{A} is denoted as $\mathbf{A} = [\mathbf{a}_1, \dots, \mathbf{a}_m]$, where \mathbf{a}_i is the i th column of \mathbf{A} . The element of a matrix \mathbf{A} at position (i, j) is denoted as a_{ij} and the diagonal of a matrix $\mathbf{A} \in \mathbb{C}^{m \times m}$ is denoted as $\text{Diag}(\mathbf{A}) = [a_{11}, \dots, a_{mm}]^T$. For the Frobenius norm of a matrix, we use $\|\cdot\|_F$ to denote it. A hermitian positive semi-definite matrix is denoted as $\mathbf{A} \succeq 0$, where $\mathbf{A} = \mathbf{A}^H$ and the eigenvalues of \mathbf{A} are real and non-negative.

2.2. Atrial electrogram impulse response model

To model the electrical propagation in epicardial tissue, we consider the cable theory and the monodomain approach, which assumes that the anisotropy ratios of the intracellular domain and the extracellular domain are equal. It has been found in the previous research that the monodomain model approximates its bidomain counterpart very well, even when the equal anisotropy assumption does not exactly hold [20–22].

We consider M electrodes that are positioned on an epicardial area of the left/right atrium. The electrodes are indexed by $m \in \{1, 2, \dots, M\}$. Fig. 1 illustrates as an example of the placement of the electrode array on different epicardial areas of the atria. These electrodes measure the changes in the extracellular potential of a group of cells that are close to the electrodes. These measurements are called epicardial electrograms.

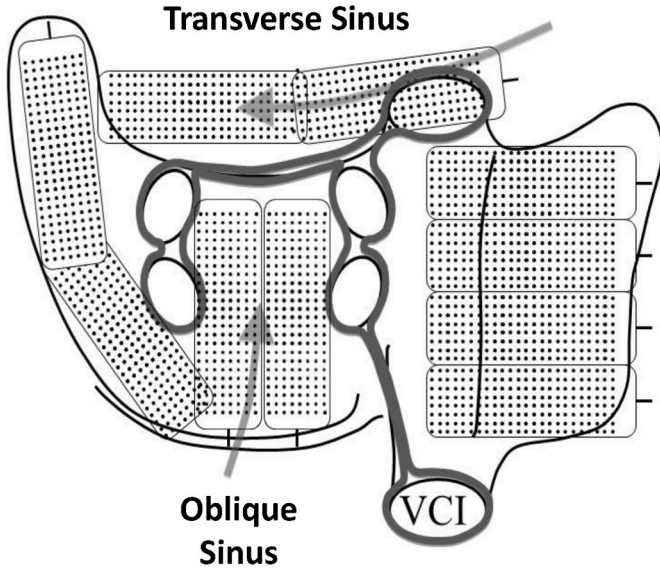


Fig. 1. The placement of the electrode array on different epicardial areas of the atria. The black dots represent the electrodes. VCI: vena cava inferior.

To represent the electrograms in a computational model, we discretize the tissue into a two-dimensional grid with N regular elements to model N cells. We use $r_{m,n}$ to denote the distance between the m th electrode and the n th cell and let $\mathbf{r}_m = \left[\frac{1}{r_{m,0}}, \frac{1}{r_{m,1}}, \dots, \frac{1}{r_{m,N-1}} \right]^T$. By stacking the action potential of all cells in a vector $\mathbf{v}(t) = [v_0(t), v_1(t), \dots, v_{N-1}(t)]^T$, the atrial electrogram recorded by the m th electrode can be modeled as [10,23].

$$y_m(t) = \frac{aS_v^{-1}}{4\pi\sigma_e} \mathbf{r}_m^T \mathbf{D}_\sigma \mathbf{v}(t), \quad (1)$$

where a represents the area of each grid element, σ_e represents the constant extra-cellular conductivity, S_v represents the cellular surface to volume ratio, and \mathbf{D}_σ represents a double differentiation operator. We consider to decompose the propagation direction of the action potential into a component in the x -direction and a component in the y -direction and denote the ratio of the conductivity in the x -direction to the conductivity in the y -direction at the n th cell position by α_n . Stacking the conductivity of all cells in the x -direction as a vector σ , and stacking the anisotropy ratio of all cells as a vector α , the operator \mathbf{D}_σ is defined as

$$\mathbf{D}_\sigma = \mathbf{D}_x \text{Diag}(\sigma) \mathbf{D}_x + \mathbf{D}_y \text{Diag}(\alpha) \text{Diag}(\sigma) \mathbf{D}_y. \quad (2)$$

Similar as in [10], we assume that all cells have the same stereotype action potential waveform once activated and take the cell with action potential $v_0(t)$ as the reference cell. The electrogram model in (1) can then be rewritten as:

$$y_m(t) = \frac{aS_v^{-1}}{4\pi\sigma_e} \mathbf{r}_m^T \mathbf{D}_\sigma \delta(t) * v_0(t), \quad (3)$$

where $\delta(t) = [\delta(t - \tau_0), \delta(t - \tau_1), \dots, \delta(t - \tau_{N-1})]^T$, with $\delta(\cdot)$ the Dirac delta function and τ_n the time delay of the n th cell with respect to the reference cell, and $*$ the convolution operator.

Let $a_m(t)$ denote the impulse response from all cells to the sensor at position m . From the model in (3), we have

$$a_m(t) = \frac{aS_v^{-1}}{4\pi\sigma_e} \mathbf{r}_m^T \mathbf{D}_\sigma \delta(t). \quad (4)$$

with this, the atrial electrogram model in (3) can be further simplified as

$$y_m(t) = a_m(t) * v_0(t). \quad (5)$$

In practice, the electrodes at the atrial area measure not only the

action potentials of the atrial cells, but also the action potentials of the ventricular cells and some noise. In this work, we only aim to estimate the parameters of the atrial tissue when atrial activity is present and ignore the ventricular activity. Denoting the noise received at the m th electrode by $u_m(t)$, the impulse response model of the noisy atrial electrogram measured by the m th electrode is given by

$$y_m(t) = a_m(t) * v_0(t) + u_m(t). \quad (6)$$

The conductivity parameters σ and the anisotropy ratio parameters α in \mathbf{D}_σ and the activation time parameters τ_n for all $n = 0, \dots, N-1$ are the parameters of interest in this work, which are all included in $a_m(t)$. Estimating these parameters from the model in (6) is complex because of the convolution operator. To simplify the problem, we transform the model to the frequency domain with the short-time Fourier transform (STFT).

2.3. Atrial electrogram CPSDM model

The time domain electrogram model can be written in the frequency domain using the STFT. Let l denote the time-frame index and k denote the frequency-bin index. In the frequency domain, the electrogram model from (6) is then given by

$$\tilde{y}_m(l, k) = \tilde{a}_m(l, k) \tilde{v}_0(l, k) + \tilde{u}_m(l, k) \quad (7)$$

where $\tilde{y}_m(l, k)$, $\tilde{a}_m(l, k)$, $\tilde{v}_0(l, k)$, and $\tilde{u}_m(l, k)$ are the STFT coefficients of $y_m(t)$, $a_m(t)$, $v_0(t)$, and $u_m(t)$, respectively.

By stacking all electrodes in a vector, the electrogram model in the frequency domain becomes

$$\tilde{\mathbf{y}}(l, k) = \tilde{\mathbf{a}}(l, k) \tilde{v}_0(l, k) + \tilde{\mathbf{u}}(l, k), \quad (8)$$

where

$$\tilde{\mathbf{y}}(l, k) = [\tilde{y}_1(l, k), \dots, \tilde{y}_M(l, k)]^T, \quad (9)$$

$$\tilde{\mathbf{u}}(l, k) = [\tilde{u}_1(l, k), \dots, \tilde{u}_M(l, k)]^T, \quad (10)$$

and

$$\tilde{\mathbf{a}}(l, k) = \left[\frac{aS_v^{-1}}{4\pi\sigma_e} \mathbf{r}_1^T \mathbf{D}_\sigma \tilde{\delta}(l, k), \dots, \frac{aS_v^{-1}}{4\pi\sigma_e} \mathbf{r}_M^T \mathbf{D}_\sigma \tilde{\delta}(l, k) \right]^T \quad (11)$$

with

$$\tilde{\delta}(l, k) = \left[\exp\left(-j \frac{2\pi f_s k}{K} \tau_0(l)\right), \dots, \exp\left(-j \frac{2\pi f_s k}{K} \tau_{N-1}(l)\right) \right]^T, \quad (12)$$

where $\tau_n(l)$ is the time delay of the n th cell with respect to the reference cell in the l th frame.

Based on (7), the cross power spectral density matrix (CPSDM) of the electrograms in the l th frame and the k th frequency bin can be expressed as

$$\begin{aligned} \Phi_y(l, k) &= E[\tilde{\mathbf{y}}(l, k) \tilde{\mathbf{y}}(l, k)^H] \\ &= \varphi(l, k) \tilde{\mathbf{a}}(l, k) \tilde{\mathbf{a}}(l, k)^H + \Phi_u(l, k), \end{aligned} \quad (13)$$

where $\varphi(l, k) = E[|\tilde{v}_0(l, k)|^2]$ is the power spectral density of the reference cell, and $\Phi_u(l, k) = \text{Diag}([q_1, \dots, q_M]^T)$ with the m th diagonal element $q_m = E[|\tilde{u}_m(l, k)|^2]$ the power spectral density of the sensor-self noise of the m th sensor, which is assumed to be uncorrelated across sensors, across time and across frequency bins.

For the CPSDM model, the unknown parameters of interest, i.e., σ and α are included in the spatial operator \mathbf{D}_σ in $\tilde{\mathbf{a}}(l, k)$ [ref. (2)], and the activation time parameters τ_n for all $n = 0, \dots, N-1$ are included in $\tilde{\delta}(l, k)$ in $\tilde{\mathbf{a}}(l, k)$.

2.4. Problem formulation

The goal of this work now is to jointly estimate the conductivity parameters σ , the anisotropy ratio parameters α , and the activation time parameters τ_n for all $n = 0, \dots, N - 1$ from the noisy CPSDM matrices $\Phi_y(l, k)$, estimated from the electrograms of multiple heart beats for all time frames.

In this problem, the number of knowns depends on the number of electrodes used for data measurements and the number of unknowns depends on the number of cells (modeled by the spatial grid elements of the tissue) given a certain number of electrodes. To make the problem solvable, the number of knowns needs to be larger than the number of unknowns. This can be confirmed by analyzing the identifiability conditions of the confirmatory factor analysis (CFA) problem. Next, we will use CFA to analyze the resolution that we can obtain with the given amount of data and estimate the target parameters.

3. Simultaneous confirmatory factor analysis for joint estimation of tissue properties

CFA has been proposed to estimate parameters to fit a hypothesized measurement model based on variance-covariance structures of the data, which can be applied to estimate the parameters in CPSDM models. Interested readers are referred to the studies in [14–17] for more details. Generally, solving the CFA problem is done by minimizing the distance between the estimated CPSDMs of the noisy measurements and the theoretical CPSDMs with respect to some free parameters while keeping the remaining parameters fixed at the given values. In most cases, this implies to solve an optimization problem with constraints to incorporate a priori knowledge of the models and parameters.

Two necessary conditions have been proposed to ensure the parameters of the CPSDM model are uniquely identifiable [17]. The *first identifiability condition* is that the number of equations should be larger than the number of unknown parameters. The number of equations depend on the given amount of data. In this problem, it depends on the number of electrodes M used in the measurement. For guaranteeing unique identifiability, the *first identifiability condition* is not enough and the *second identifiability condition* is needed. This condition states the number of parameters in the CPSDM model that at least need to be fixed to have a unique solution.

3.1. Simultaneous CFA problem for joint estimation in multiple frequencies and multiple heart beats

In [12], we have adapted the CFA method to estimate the cardiac tissue conductivity parameters and the anisotropy ratio parameters from the CPSDM model using a single heart beat. We now apply the CFA to estimate interested parameters in this work, i.e., the conductivity, anisotropy ratio, and activation time parameters from the CPSDM model in (13) using multiple heart beats.

To increase the robustness of the estimation, we put some constraints on the parameters exploiting some a priori knowledge. The power spectral density of the reference cell φ is fixed by a known constant $\hat{\varphi}$, which is obtained based on the mathematical model of the action potential of an atrial cell. For the reference cell with index zero, the activation time $\tau_0(l) = 0$ for all heart beats (for all l). Based on the assumption that the conductivity σ , the anisotropy ratio α and the activation time τ_n in different frequencies are roughly constant, we estimate these parameters simultaneously in multiple frequencies to increase the ratio of known-to-unknown variables when estimating the conductivity parameters using CPSDMs of noisy atrial electrograms. Moreover, we take into account multiple heart beats, since the conductivity σ and the anisotropy ratio α can also be assumed constant across multiple heart beats. By using multiple heart beats, the *first identifiability condition* can be easier satisfied, and the estimation error may be further reduced since waves coming from varying directions

illuminate the tissue from various viewpoints. Note that the activation time parameters are constant across frequencies but differ across heart beats. The simultaneous CFA (SCFA) problem formulation to jointly estimate the parameters in multiple frequencies and multiple heart beats is given by

$$\begin{aligned} & \min_{\sigma, \alpha, \{\Phi_u(k, l)\}, \{\tau_n(l)\}, n=0, \dots, N-1} \sum_{\forall k \in S_f, \forall l \in S_l} F(\hat{\Phi}_y(k, l), \Phi_y(k, l)) \\ & \text{s.t.} \quad \Phi_y(k, l) = \tilde{\mathbf{a}}(k, l) \varphi(k, l) \tilde{\mathbf{a}}^H(k, l) + \Phi_u(k, l), \\ & \quad \tilde{\mathbf{a}}(k, l) = [Q \mathbf{r}_1^T \mathbf{D}_\sigma \tilde{\delta}(k, l), \dots, Q \mathbf{r}_M^T \mathbf{D}_\sigma \tilde{\delta}(k, l)]^T, \\ & \quad \mathbf{D}_\sigma = \mathbf{D}_x \text{Diag}(\sigma) \mathbf{D}_x + \mathbf{D}_y \text{Diag}(\alpha) \text{Diag}(\sigma) \mathbf{D}_y, \\ & \quad \tilde{\delta}(k, l) = \left[\exp\left(-\frac{j2\pi f_s k}{K} \tau_0(l)\right), \dots, \right. \\ & \quad \quad \left. \exp\left(-\frac{j2\pi f_s k}{K} \tau_{N-1}(l)\right) \right], \\ & \quad \Phi_u(k, l) = \text{Diag}[q_1(k, l), q_2(k, l), \dots, q_M(k, l)], \\ & \quad q_m(k, l) \geq 0, m = 1, 2, \dots, M, \\ & \quad \varphi(k, l) = \hat{\varphi}(k, l), \\ & \quad 0 < \alpha \leq \alpha_{\text{upper}}, \\ & \quad 0 \leq \sigma \leq \sigma_{\text{upper}}, \\ & \quad \tau_0(l) = 0, \\ & \quad \tau_{\text{low}} \leq \tau_n(l) \leq \tau_{\text{upper}}, n = 1, \dots, N-1, \end{aligned} \quad (14)$$

where $F(\hat{\Phi}_y, \Phi_y)$ is a cost function such as the maximum likelihood, least square, or generalized least square, and where the constraints are used to incorporate model knowledge, for example the a priori knowledge from (13) and incorporating the knowledge that Φ_u is diagonal and positive definite. Constraints are also put on the target parameters, which are expressed by the last four constraints in (14), where α_{upper} and σ_{upper} are respectively the real valued upper bounds on the anisotropy ratio and the conductivity parameters which are selected based on the previous research on the atrial tissue, and τ_{low} and τ_{upper} are respectively the lower and upper bounds of activation time that are set by reasonable values. For the loss function in (14), we consider to use the least square cost function, which is given by

$$F(\hat{\Phi}_y, \Phi_y) = \frac{1}{2} \|\hat{\Phi}_y - \Phi_y\|_F^2, \quad (15)$$

for $\forall k \in S_f, \forall l \in S_l$, where $S_f = \{k_1, \dots, k_N\}$ is the set of the frequency indices and $S_l = \{l_1, \dots, l_N\}$ is the set of the heart beats for conductivity and activation time estimation. Note that the problem in (14) is not convex and may have multiple local minima.

3.2. Identifiability conditions of the SCFA problem

Prior to estimating the target parameters in this CFA problem, we first analyze what resolution we can obtain given M electrodes. This can be achieved by analyzing the two identifiability conditions of the SCFA problem. To analyze whether the *first identifiability condition* is satisfied, we need to calculate the number of knowns and unknowns in (14). Since the noisy CPSDM estimated for M electrodes in one frequency band and one heart beat is symmetric, there are M^2 real valued knowns due to $\Phi_y(k, l)$ in total. (Note that the main diagonal elements of $\Phi_y(k, l)$ are real values while others are complex values). When considering $|S_f|$ frequency bands and $|S_l|$ heart beats, the number of knowns due to the noisy CPSDMs of M electrodes in $|S_f|$ frequency bands and $|S_l|$ heart beats is $|S_f| |S_l| M^2$. The number of unknowns due to σ in \mathbf{D}_σ is N , due to α

in \mathbf{D}_σ is N , due to $\tau_n(n = 1, \dots, N - 1)$ is $|S_l|(N - 1)$, and due to Φ_u is $|S_l|S_fM$. Therefore, the *first identifiability condition* is

$$|S_l||S_f|M^2 \geq 2N + |S_l|(N - 1) + |S_l||S_f|M, \quad (16)$$

which means that the number of cells N for which we can estimate the desired parameters is constrained by

$$N \leq \frac{|S_l||S_f|(M^2 - M) + |S_l|}{2 + |S_l|}. \quad (17)$$

we can see that using multiple frequencies or/and multiple heart beats, i. e., $|S_l| > 1$ or/and $|S_f| > 1$, the *first identifiability condition* can be satisfied with less sensors.

The *second identifiability condition* requires that at least r^2 parameters in $\tilde{\mathbf{a}}$ and φ in the CPSDM model in (13) need to be fixed, where r represents the number of sources that trigger the atrial activity in the cardiac tissue [12]. According to the *second identifiability condition*, we need r^2 independent restrictions on $\tilde{\mathbf{a}}$ and φ . In this work we consider only a single source, therefore $r^2 = 1$. Since we have fixed the value of φ in the constraint, the *second identifiability condition* is always satisfied.

3.3. Practical consideration

Due to the large number of cells in the tissue, the *first identifiability condition* cannot be satisfied if we estimate parameters at the finest resolution, that is, estimating the parameters for each cell. To ease this problem we considered groups of cells and used the center cell of the group to represent the group.

Let N denote the number of cell groups and let R represent the resolution scale compared to the number of electrodes M , then $N = RM$. The *first identifiability condition* in (17) can be rewritten using R as

$$RM \leq \frac{|S_l||S_f|(M^2 - M) + |S_l|}{2 + |S_l|}. \quad (18)$$

which means that the highest resolution scale that can be obtained given M electrodes is

$$R = \frac{|S_l||S_f|(M^2 - M) + |S_l|}{(2 + |S_l|)M}. \quad (19)$$

By reducing the resolution scale R at which we estimate the parameters, that is, increasing the number of cells per group, we can reduce the number of unknowns and increase the ratio of the number of equations to the number of unknowns, which then satisfies easier the *first identifiability condition*. However, note that reducing the resolution scale R will reduce the model accuracy and increase the model-mismatch error compared to using the actual cells.

The parameters are finally obtained by solving the non-convex optimization problem in (14). In this work, we used the MATLAB optimization toolbox to solve this problem, which is based on a combination of the methods in [24–26].

4. Experiments on the simulated data

In this section, we evaluate the performance of the proposed methods on simulated data. We first introduce the data generation based on the mathematical model and then evaluate the joint estimation of the conductivity, anisotropy ratio, and activation time using one heart beat and multiple heart beats, respectively. The results of the proposed method are compared with our previously proposed SCFA method from [12], which assumed the activation time parameters were known and in the end were estimated by the steepest descent approach from [19] before conductivity estimation. For convenience, we use SCFA1 to represent the method in [12] and SCFA2 to represent the method proposed in this paper. The algorithms are first tested on two-dimensional simulated tissue and then on three-dimensional simulated tissue.

4.1. Generation of two-dimensional simulated data

4.1.1. Model of atrial cells

To generate the atrial electrograms for evaluation, we first model individual cells and then integrated these cells to form the tissue. To generate realistic action potentials, properties and ionic mechanisms in atrial cells need to be considered in the computational cell model. In this work, we use the Courtemanche model proposed in [27] to model the atrial cells.

4.1.2. Types of two-dimensional tissue

Two-dimensional tissues with different conductivity settings are considered in the simulations to test the performance, including three types of tissues:

- (i) inhomogeneous tissue with two areas of conduction block and the area outside the conduction block is homogeneous and isotropic with conductivity $\sigma_n = 1.1$ mS/cm for all n and with anisotropic ratio $\alpha_n = 1$ for all n ;
- (ii) inhomogeneous tissue with one area of conduction block and the area outside the conduction block has a smooth variation in conductivity, varying from 0.77 mS/cm to 1.1 mS/cm and its anisotropic ratio $\alpha_n = 0.4$ for all n ;
- (iii) inhomogeneous tissue with two areas of conduction block and the area outside the conduction block has a higher variation in conductivity than (ii) which varies from 0.75 mS/cm to 1.3 mS/cm and its anisotropic ratio α_n changes from 0.9 to 0.5 from left to right.

4.1.3. Simulation protocol

Tissues are discretized into 90×90 regular grid points to model the cells. The cell-to-cell distance is 0.02 cm. At the beginning, all the cells are at their resting status with the initial conditions as set in Ref. [27]. Then, a train of stimulus with a basic cycle length of 1000 ms is applied to the source cells in the tissue during 5 s. The stimulus current is $I_{st} = 200 \mu\text{A}$ with a duration of 0.5 ms. Once the source cells are activated, they generate and conduct the impulses to their neighbors, causing the spread of excitation through the tissue. The electrical waves in different heart beats are assumed to be originating from slightly different directions, which is implemented by applying the stimulus at different positions of the tissue.

4.1.4. Calculation of action potentials and electrograms

The basic equation to calculate the transmembrane potentials of the cells is

$$C \frac{\partial v_n(t)}{\partial t} = I_{tm,n}(t) + I_{st,n}(t) - I_{ion,n}(t, v_n(t)) \quad (20)$$

where $v_n(t)$ is the transmembrane potential of the n th cell, C is the membrane capacitance, $I_{st,n}(t)$ is the stimulus current, $I_{ion,n}(t, v_n(t))$ is the ionic current, and $I_{tm,n}(t)$ is the cell-to-cell transmembrane current per unit area that accounts for the spatial evolution of the action potential. By discretizing the tissue into a regular lattice, the reaction-diffusion equation in (20) can be solved using the finite difference method [28]. This is based on the assumption that the tissue surface is flat, which is reasonable when taking into account a small tissue area. Since the electrical wave should not propagate further than the tissue boundaries, the no-flux boundary conditions is considered. After solving (20) using forward Euler's method with a time step of 0.05 ms, we obtain the action potential at every grid point of the tissue. The moment when the action potential of a cell reaches the threshold of -40 mV is considered as the cell's activation time. After calculating the action potentials of all cells, the electrograms are generated using the mathematical model in (1). The noisy electrograms are then generated by adding Gaussian noise to the clean electrograms to simulate sensor self noise. The signal-to-noise

ratio (SNR) is set at 50 dB. In the numerical experiments, we assume the fiber is aligned along the x-axis and simply choose $\alpha_{\text{upper}} = 1$. The values of other parameters used for the experiments are summarized in Table 1.

Fig. 2 shows an example of the experimental setup, the generated electrograms and the activation time maps of the heart beats. Fig. 2(a) shows tissue as having the two areas of conduction block with a 5×5 electrode array placed on the center of the tissue. The two blue lines represent the two areas of conduction block. The cells outside the areas of conduction block have a conductivity of 1.1 mS/cm. The nine red points numbered from one to nine represent the simulated source positions of the nine heart beats, respectively, where an external stimulus current of $I_{st} = 200 \mu\text{A}$ is applied to trigger the electrical activity in the tissue. Note that for each heart beat there is only one source to drive the propagation of the wave. Fig. 2(b) plots the generated electrograms of the nine heart beats measured by the electrode array in Fig. 2(a). We can see the small differences between these heart beats. Fig. 2(c) and (d) plot the activation time maps of the tissue area with 45×45 cells in the central part of the tissue boxed in Fig. 2(a) when applying the stimulus at position '1' and position '3' in Fig. 2(a), respectively.

4.2. Evaluation on two-dimensional simulated data

To quantify the estimation performance, we calculate the MSE of the conductivity parameters and the MSE of the activation time parameters. The conductivity parameters in the y-direction (the transverse direction) σ_{yy} can be obtained after estimating the conductivity parameters in x-direction (the longitudinal direction) σ_{xx} and the anisotropy ratio α . The longitudinal conductivity at the location of the n th cell, i.e., $\sigma_{yy,n}$, is equal to $\sigma_{xx,n} \cdot \alpha_n$, where $\sigma_{yy,n}$, $\sigma_{xx,n}$ and α_n are the n th elements of the vector σ_{yy} , σ_{xx} and α_n . Then we calculate the MSE for the estimation of the conductivity parameters by

$$\text{Err}_c = \frac{\|\sigma_{xx} - \hat{\sigma}_{xx}\|^2 + \|\sigma_{yy} - \hat{\sigma}_{yy}\|^2}{2N}, \quad (21)$$

where N represents the number of cell groups, σ_{xx} and σ_{yy} represents the real longitudinal and transverse conductivity parameters, and $\hat{\sigma}_{xx}$ and $\hat{\sigma}_{yy}$ represents their estimates, respectively.

The MSE of the estimated activation time parameters for the l th time frame (heart beat) is calculated by

$$\text{Err}_a(l) = \frac{1}{N} \sum_{n=0}^{N-1} (\tau_n(l) - \hat{\tau}_n(l))^2, \quad (22)$$

where τ_n and $\hat{\tau}_n$ represent the real and estimated activation time parameters in ms, respectively.

We first compare the parameters estimated by SCFA1 and SCFA2 using a single heart beat. Table 2 shows the estimation errors for different heart beats. It can be seen that for all the tissue examples the estimation errors of the conductivity and the activation time parameters both decrease when using the joint estimation method SCFA2 proposed in this work. Moreover, it is clear that the estimation performance varies with the source position. This is due to the interplay between the origin of the wave (i.e., the source position) and the local conductivity. Compared with SCFA1, the average MSE of conductivity parameter per cell obtained by SCFA2 decreases from 0.0413 mS/cm to 0.0359 mS/cm for tissue type (i), from 0.0297 mS/cm to 0.0241 mS/cm for tissue type

(ii), and from 0.0585 mS/cm to 0.0560 mS/cm for tissue type (iii).

The estimation of the activation time is also improved by using the joint estimation method. The electrical wave propagates fast across the tissue. The SCFA1 method uses the steepest descent method to estimate the activation time parameters of the 45×45 cells per tissue. The MSE of the activation time parameter per cell is 0.8607 ms^2 , 1.2212 ms^2 , and 1.2865 ms^2 for tissue type (i), type (ii), and type (iii), respectively. Unlike SCFA1, the SCFA2 method jointly estimates all the parameters and the MSE of the activation time parameter per cell decreases to 0.8490 ms^2 , 1.1991 ms^2 , and 1.2422 ms^2 for tissue type (i), type (ii), and type (iii), respectively. Although the MSE decrease for per cell is small, at the high speed of wave propagation in tissue this difference can be significant.

We then study the use of multiple heart beats to estimate the parameters. We start from using two heart beats and test different combinations of two heart beats, for example, combining heart beat '1' with each of the heart beats '2', '3', ..., '9', respectively, i.e., heart beats '1'&'2', '1'&'3', ..., '1'&'9'. We here compare the estimation performance using three different methods, that are: 1) SCFA1 using one heart beat, 2) SCFA2 using one heart beat, and 3) SCFA2 using two heart beats. Fig. 3 shows the resulting estimation errors of the conductivity parameters and activation time parameters. The estimation errors of the first two methods are obtained by calculating the errors for the conductivity and activation time per heart beat and averaging these across the two heart beats. The estimation errors of SCFA2 using two heart beats are calculated directly. Fig. 3(a) and (b) respectively show the estimation errors of the conductivity parameters and the activation time parameters on the three tissue examples using different methods. We here use $\bar{\text{Err}}_c$ and $\bar{\text{Err}}_a$ to denote the estimation errors of the conductivity parameters and the activation time parameters, respectively. We can see that for all tissue examples, SCFA2 achieves better performance than SCFA1 and the estimation errors of the parameters are reduced by combining two different heart beats and estimating the parameters jointly. These results support our hypothesis that the electrical waves in different heart beats can "illuminate" the tissue from different directions and provide useful information for the tissue parameter estimation.

We then increase the number of heart beats for estimation using SCFA2. Fig. 4(a) and Fig. 4(b) respectively plot the estimation errors of the conductivity parameters and the activation time parameters on the three tissue types from using one heart beat up to nine heart beats. From Fig. 4(a), we see that for all the tissue examples the estimation error of the conductivity parameters first decreases and then tends to stabilize with the increase of the number of heart beats. We can also find that tissue type (iii) needs more heart beats to achieve good results since it has a more complicated underlying structure. However, we also see that it has the largest relative decrease in estimation error when going from one to multiple heart beats. This can also be explained by the more complex structure, where a larger benefit is obtained by combining heart beats originating from different directions. From Fig. 4(b), we find that using multiple heart beats helps to improve the estimation of the activation time parameters, and always performs better than the steepest descent method. However, the improvement of the activation time estimation due to the increase of heart beats is less obvious compared to the conductivity estimation in Fig. 4(a). This might be because the activation time parameters change across different heart beats, while the conductivity parameters are shared across different heart beats. In addition, the increase of the unknown parameters due to the increase of the number of heart beats makes it more challenging to find the optimal solution in the non-convex optimization problem.

In Fig. 5, we show examples of the real and estimated conductivity maps obtained with SCFA1 using one heart beat, SCFA2 using one heart beat, two heart beats, and three heart beats. Since the longitudinal conductivity is equal to the transverse conductivity for tissue type (i) and the estimation results are similar in the two directions, we only show here the conductivity maps in the longitudinal direction for tissue

Table 1
Summary of parameters used in the experiments.

Parameters	Definition	Value
T	time-frame length	1000 samples
ov_T	overlapping of time-frame	20%
f_s	sampling frequency	1 kHz
C	membrane capacity	$1 \mu\text{F}/\text{cm}^2$
S_v	cellular surface to volume ratio	$0.24 \mu\text{m}^{-1}$
σ_{upper}	maximum conductivity of a cell	2 mS/cm

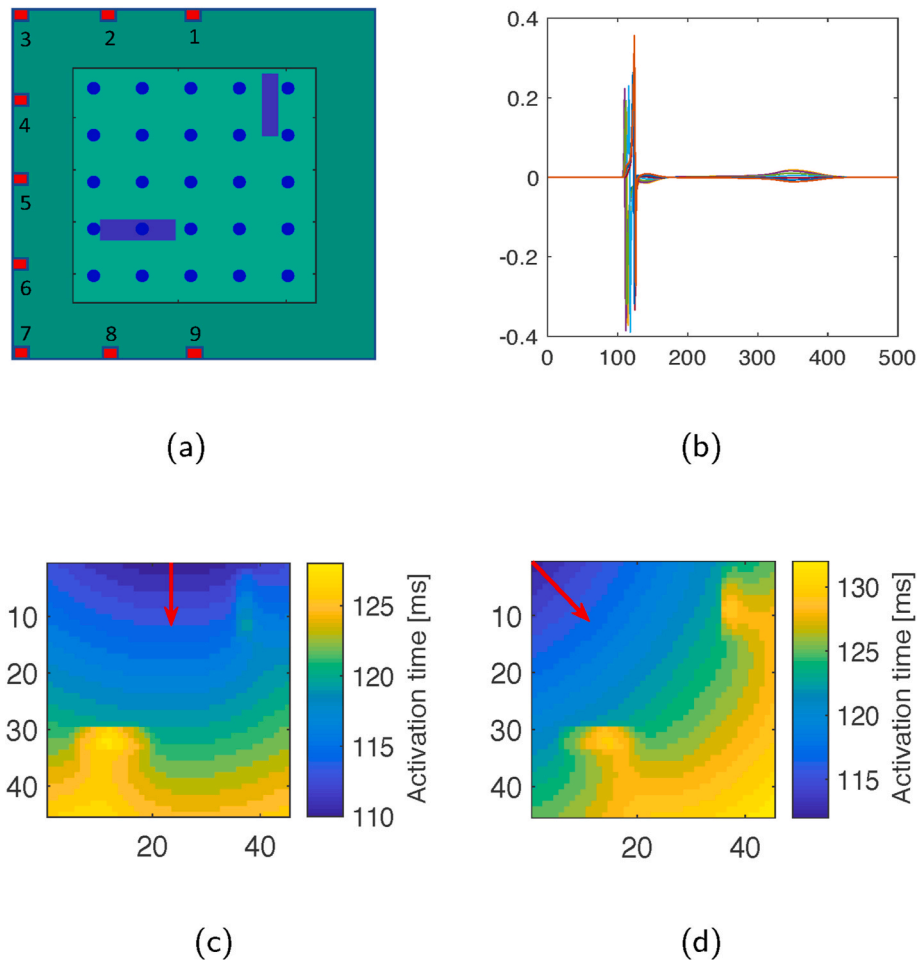


Fig. 2. An example of the tissue, the generated electrograms and activation time maps. (a) Tissue with two areas of blocks. The 5×5 blue points represent the 5×5 electrodes and the two blue lines represent the two areas of block. (b) electrograms of nine heart beats; (c) activation time map of the heart beat when applying the stimulus at position ‘1’ in (a); (d) activation time map of the heart beat when applying the stimulus at position ‘3’ in (a).

Table 2

Comparison of estimation errors with different methods.

Heart beats	Tissue Type (i)				Tissue Type (ii)				Tissue Type (iii)			
	Err _c (SCFA1)	Err _c (SCFA2)	Err _a (SCFA1)	Err _a (SCFA2)	Err _c (SCFA1)	Err _c (SCFA2)	Err _a (SCFA1)	Err _a (SCFA2)	Err _c (SCFA1)	Err _c (SCFA2)	Err _a (SCFA1)	Err _a (SCFA2)
1	0.0435	0.0384	1.0318	1.0198	0.0322	0.0273	1.0752	1.0502	0.0866	0.0861	1.5108	1.3719
2	0.0441	0.0360	0.6643	0.6480	0.0276	0.0236	1.0460	1.0142	0.0706	0.0672	1.1976	1.0890
3	0.0399	0.0337	0.6748	0.6674	0.0301	0.0233	1.4008	1.3470	0.0558	0.0579	1.6209	1.5945
4	0.0397	0.0342	0.8785	0.8598	0.0322	0.0212	0.6459	0.6262	0.0506	0.0462	0.9196	0.8440
5	0.0386	0.0334	0.9985	0.9783	0.0299	0.0215	0.4763	0.4470	0.0509	0.0477	1.5565	1.5558
6	0.0385	0.0343	0.7177	0.7010	0.0284	0.0216	0.6137	0.6030	0.0533	0.0480	0.5640	0.5601
7	0.0381	0.0360	1.2966	1.2925	0.0272	0.0216	1.7445	1.7356	0.0480	0.0482	1.2185	1.1977
8	0.0442	0.0386	0.7007	0.6944	0.0272	0.0273	1.5225	1.5130	0.0555	0.0504	2.0798	2.0526
9	0.0455	0.0388	0.7837	0.7798	0.0329	0.0294	2.4660	2.4561	0.0539	0.0518	0.9106	0.9103
Avg.	0.0413	0.0359	0.8607	0.8490	0.0297	0.0241	1.2212	1.1991	0.0585	0.0560	1.2865	1.2422

type (i). For tissue types (ii) and (iii), we show the conductivity maps in both the longitudinal and transverse directions. Comparing the results of SCFA1 and SCFA2 using one heart beat, we can see that SCFA2 achieves better estimation than SCFA1, which implies that improving the estimation of activation time helps to improve the estimation of the conductivity. Comparing the results of using one heart beat to the results of using two heart beats by SCFA2, we see that combining multiple heart beats obviously improves the estimation. From the estimated conductivity maps of tissue type (ii) in Fig. 5, we find that the algorithm also works well when there is a smooth variation in the conductivity maps.

However, the estimated conductivity maps seem less accurate for more heterogeneous examples (iii), mainly in case of non-constant anisotropy ratios. This could be a consequence of the fixed stereotype waveform for all cells.

From the simulation results, we here have some interesting findings on the conductivity estimation. For all tissue examples, we find that the combination of the waves from top and top left achieve a different conductivity map compared to the combination of the waves from top and left, which suggests that the propagation direction of the wave affects the estimation results. From the visualized examples in Fig. 5, we

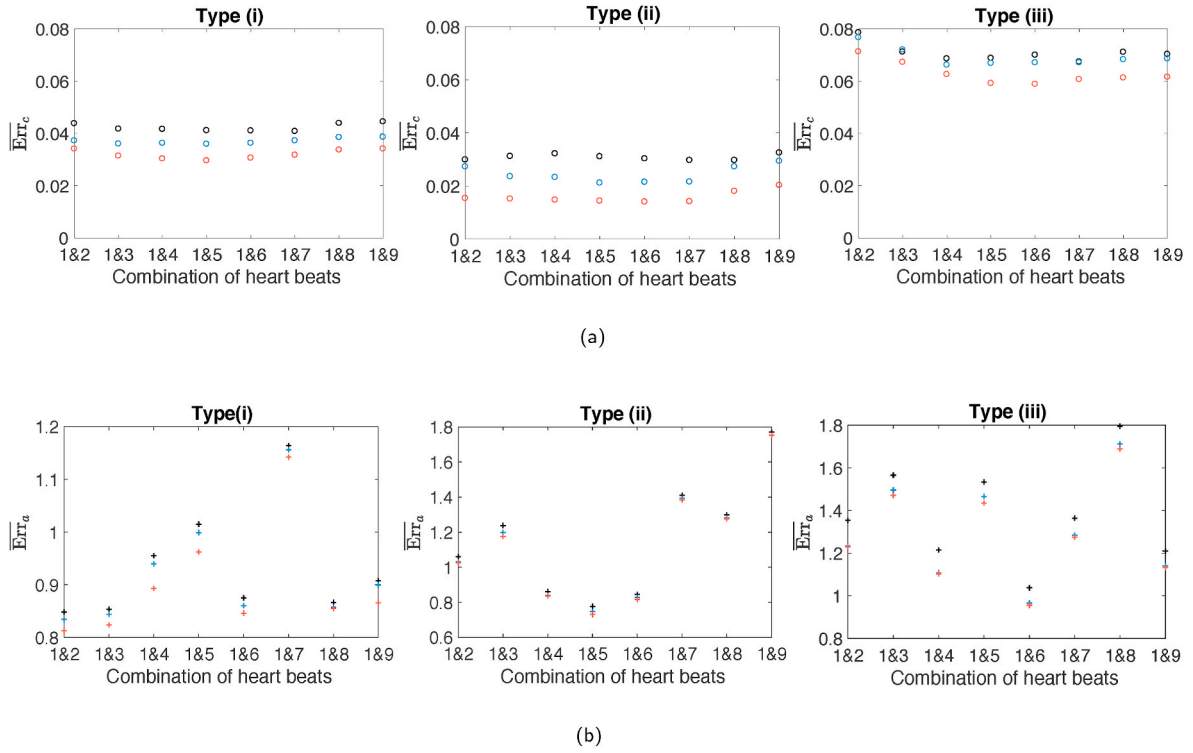


Fig. 3. Estimation errors of conductivity parameters (a) and activation time parameters (b). The SCFA2 method achieves better performance than the SCFA1 method and the estimation errors of the parameters are further reduced by combining two different heart beats and jointly estimating the parameters.

can see that using the wave from the left helps to estimate the longitudinal conduction block as the time delay at the position of the block is more obvious when the wave is propagating from the left. Similarly, using the wave from the top is good for estimating the transverse conduction block. In addition, the readers may find that in tissue example (i), the conduction block in the transverse direction is better estimated than the longitudinal direction. This is because the electrode is exactly positioned on the conduction block in the transverse direction, while this is not the case for the conduction block in the longitudinal direction and the cells close to the electrode have a bigger impact on the electrograms.

For comparison, we also provide in Fig. 6 the estimated conduction velocity (CV) maps [11], which are commonly used in the literature for analysis of conduction block in cardiac tissue. We see that the estimation of CV is significantly affected by the propagating directions of the electrical waves and that the areas of conduction block indicated by the conduction velocity maps are less accurate than those found using our estimated conductivity maps in Fig. 5. Unlike the proposed method, CV does not measure conductivity but only measures the local velocity of the action potential propagation. Although the estimation of the CV method and the proposed method can both be affected by the propagation directions of the waves, CV is less reliable for localizing the abnormal areas in tissue. Moreover, the proposed method can make use of the spatial correlation of the multi-electrode data and utilize the information from multiple heart beats, which helps to estimate the tissue properties and thus better localizes the areas of the conduction block. This comparison further shows the superiority of the proposed method in this work.

Based on these analyses, we find that the conductivity estimation is affected by many factors such as the estimation of the activation time parameters, the propagation direction of the electrical wave in a heart beat, the positions of the electrodes, and the underlying structure of the tissue. Since the underlying structure of the tissue is unknown and the relative positions of the electrodes to the cells are random, we cannot control these two factors in practice. To improve estimation of the

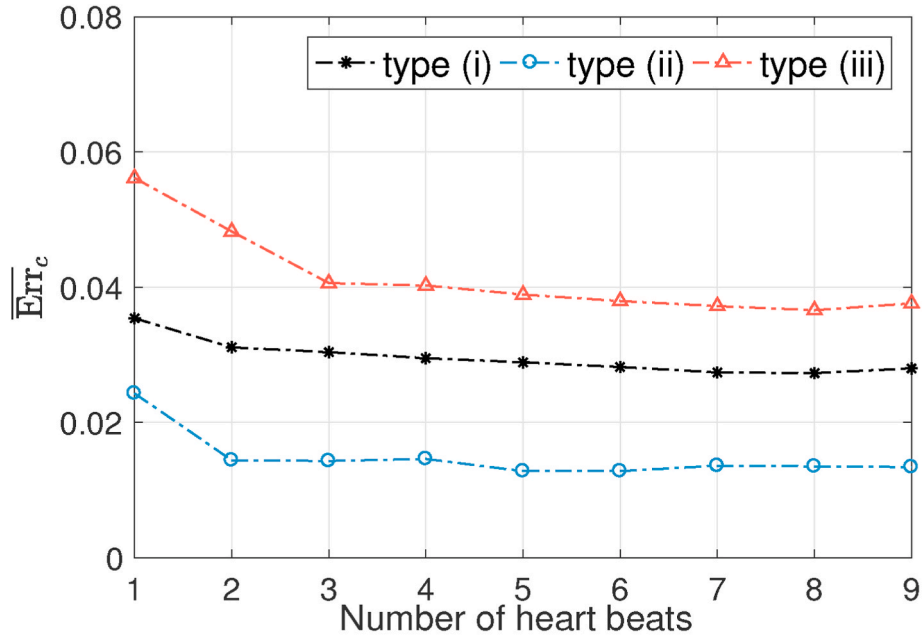
conductivity parameters, it thus obviously helps to combine multiple heart beats to get more useful information and try to improve the estimation of the activation time parameters.

4.3. Generation of three-dimensional simulated data

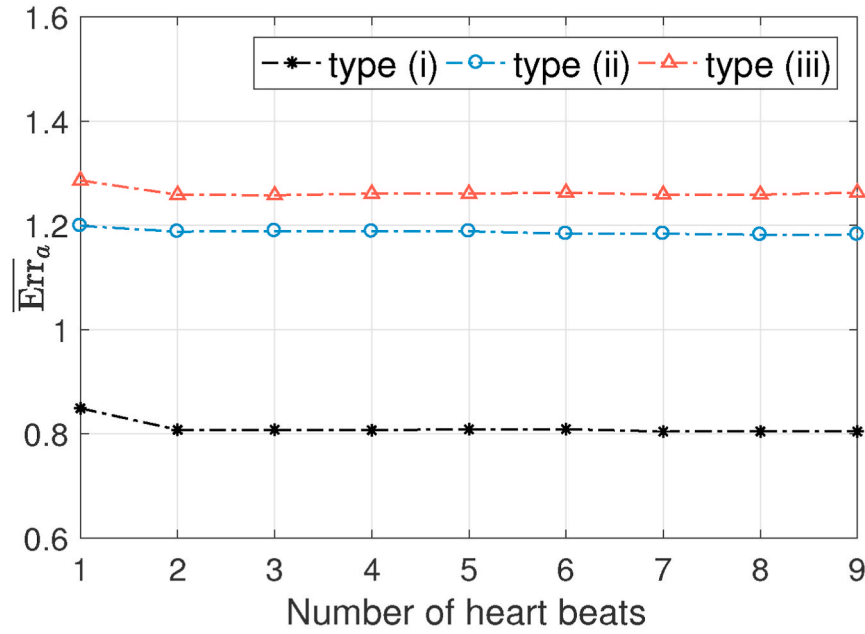
Since real tissue is three-dimensional, to evaluate the proposed algorithm with even more realistic simulations, we generate in this section three-dimensional simulated data by simulating several layers of cells to simulate the effects of three-dimensional tissue. Real tissue has many layers of cells in practice. In Section 5 we will further test the algorithm with real tissue that effectively has many layers. However, with real tissue we do not know the truth of the tissue parameters. To have a computational feasible simulation and still simulate the effect of three-dimensional tissue, we use in this section a three-layer tissue to come close to a three-dimensional simulation where we know the truth.

To generate the three-dimensional simulation data, we still use the same cell model introduced in section 4.1.1. In our model, we only consider the conductivities in the x-direction (longitudinal direction) and the y-direction (transverse direction), i.e., $\sigma_{xx,n}$ and $\sigma_{yy,n}$, and the anisotropy ratio of the conductivities in the transverse direction to the longitudinal direction to be estimated is $\alpha_n = \sigma_{yy,n}/\sigma_{xx,n}$. To simulate multiple layer tissues, we further take into account the conductivity in the z-direction that is perpendicular to the x-y plane and denote it as $\sigma_{zz,n}$ at the n th cell position. Two types of three-layer tissue are simulated taking into account equal conductivities in each layer, including:

- (i) three-layer tissue with one area of conduction block in each layer. The area outside the conduction block has a smooth variation in conductivity, varying from 0.77 mS/cm to 1.1 mS/cm. For each layer, the anisotropy ratio in our model, i.e., α_n , is set to 0.4. For the conductivities in the z-direction, we consider $\sigma_{zz,n}/\sigma_{xx,n} = 0.3$ for all n .
- (ii) three-layer tissue with two areas of conduction block in each layer. The area outside the conduction block has a higher



(a)



(b)

Fig. 4. Estimation errors of conductivity parameters (a) and activation time parameters (b) obtained by SCFA2 using different number of heart beats.

variation in conductivity than (i) which varies from 0.52 mS/cm to 1.1 mS/cm and its anisotropic ratio changes from 0.8 to 0.4 from left to right. For the conductivities in the z -direction, we consider $\sigma_{zz,n}/\sigma_{xx,n} = 0.5$ for all n .

We then use the same simulation protocol described in Section 4.1.3

to generate the cell action potentials. To generate the action potentials in these three-layer tissues, the stimuli are applied to all layers at the same positions with respect to the x - y plane. Five different positions are considered to generate five heart beats.

Fig. 7 illustrates the simulation of the three-dimensional tissues. Taking tissue (i) as an example, Fig. 7(a) and (b) show the conductivity

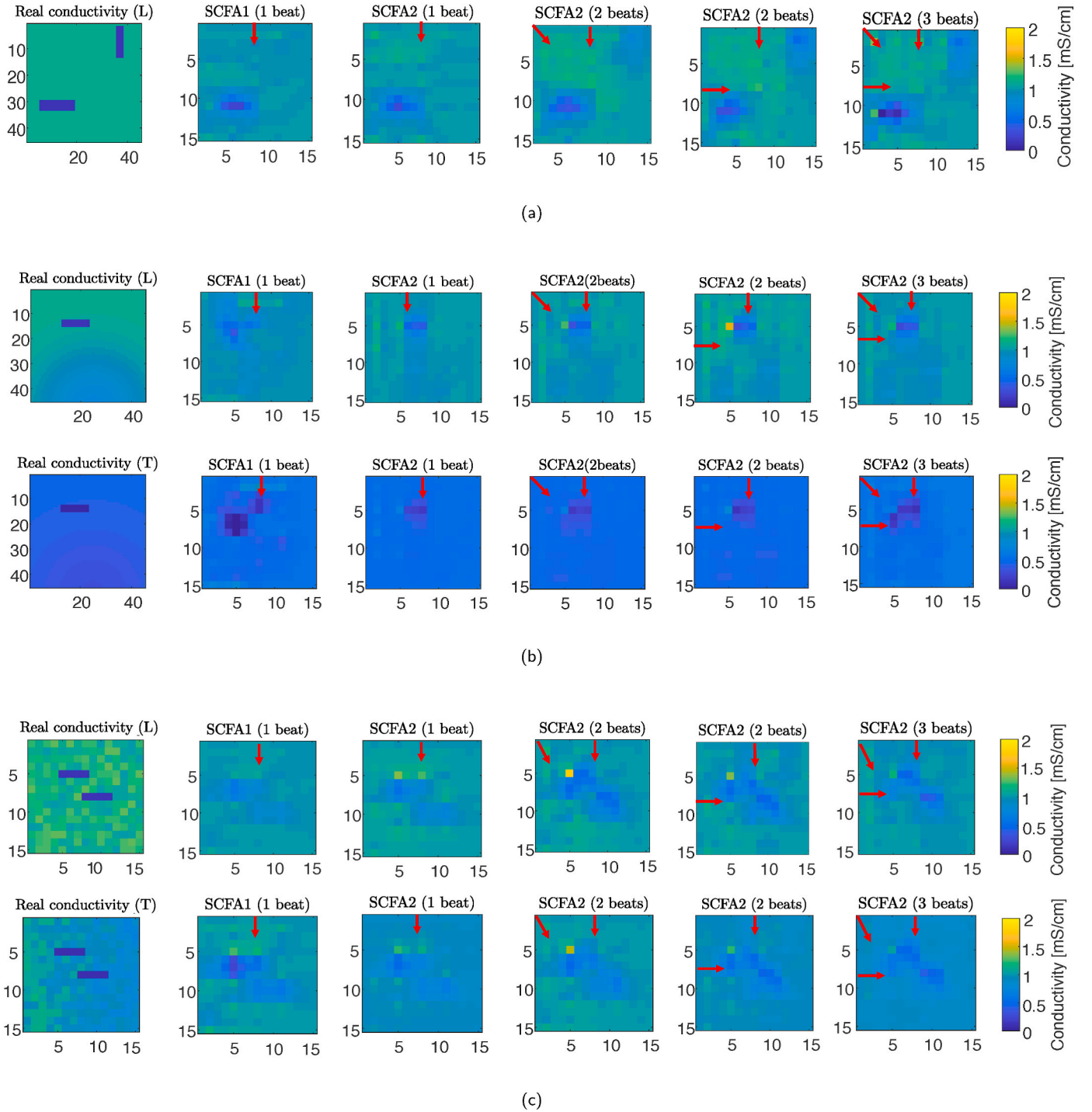


Fig. 5. Examples of the real conductivity maps and the estimated conductivity maps. The subfigures in the first column show the real conductivity maps and the subfigures in other columns show the estimated conductivity maps, which are obtained using different methods, including SCFA1 using one heart beat, SCFA2 using one heart beat, two heart beats, and three heart beats. The red arrow on the map represents the propagation direction of the wave in the heart beat. The number of arrows indicates the number of heart beats used in the estimation. (a) Longitudinal (L) conductivity maps for tissue types (i); (b) Longitudinal (L) and transverse (T) conductivity maps for tissue types (ii); (c) Longitudinal (L) and transverse (T) conductivity maps for tissue types (iii).

maps in the x-direction and the y-direction of tissue (i), respectively. We consider an electrode array with 25 electrodes placed on the top layer of the tissue to generate the multi-electrode electrograms. Both uniform and non-uniform distribution of the electrodes are considered, as shown in Fig. 7(c) and (d). Compared to the uniform placement of the electrodes, the distribution of the electrodes is more random in the non-uniform placement of the electrodes. Especially, the relative positions of the conduction blocks and the electrodes in two placements are

different such that we can test the algorithm under different difficulty levels of detecting the areas of conduction blocks. Taking Tissue (i) as an example, Fig. 7(c) and (d) show the uniform and non-uniform placement of the electrodes on top of this tissue. We see that in Fig. 7(c) there are two electrodes exactly placed on top of the conduction block, while in Fig. 7(d) they are not on top of the conduction block. As we know the cells which are closer to the electrodes contribute more to the electrograms, detecting the area of conduction block would be more

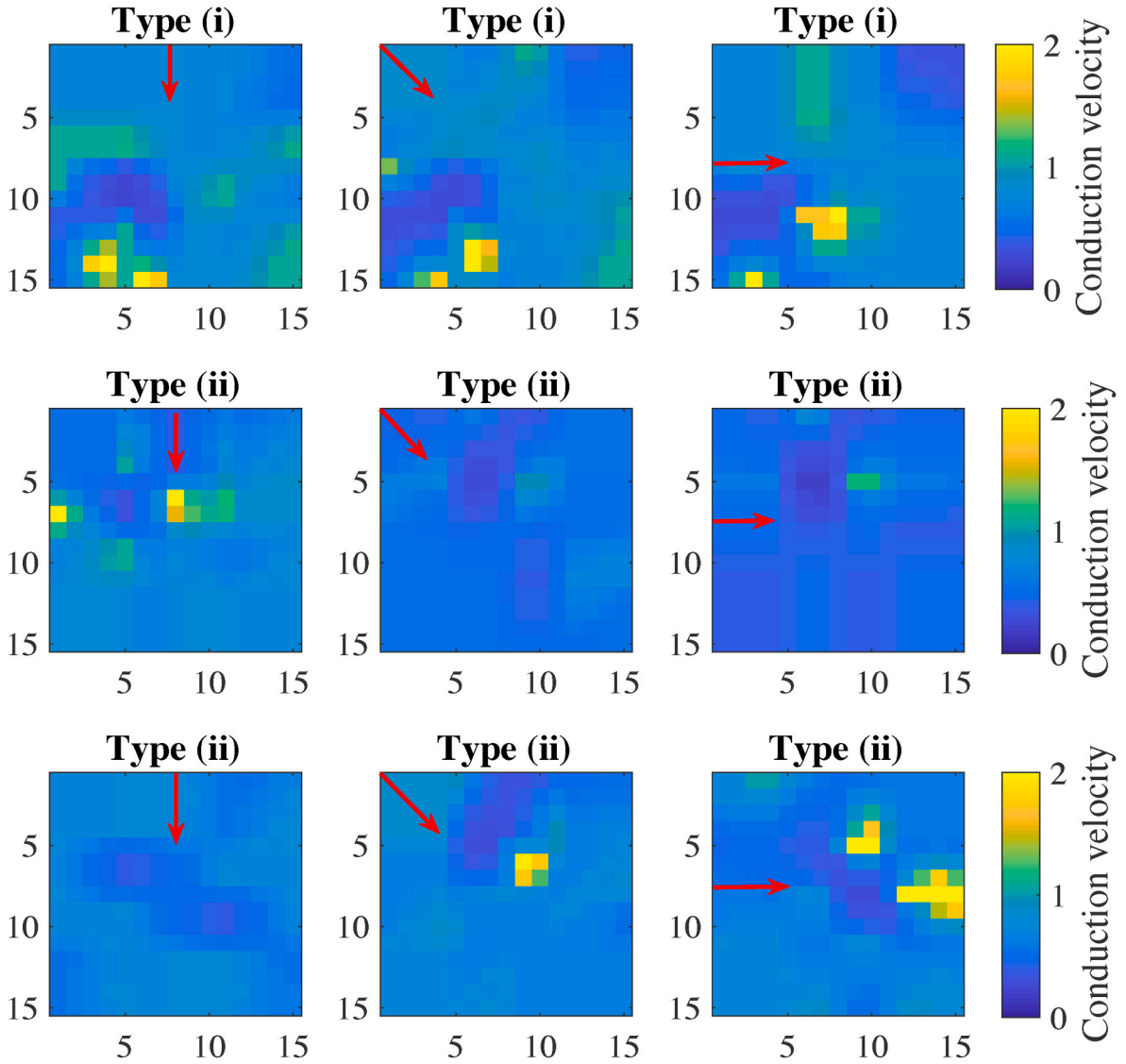


Fig. 6. Examples of the estimated conduction velocity maps for the three type of tissue. The red arrow on the map represents the propagation direction of the electrical wave in the heart beat.

challenging with the non-uniform placement of the electrodes. Fig. 7(e) shows the 3D plot of the action potential propagation in tissue (i) when $t = 200$ ms when the stimuli is applied at position '1' in Fig. 7(c).

4.4. Evaluation on three-dimensional simulated data

We now use the SCFA1 and the SCFA2 to estimate the parameters of the simulated 3D tissues. To quantify the estimation performance, we calculate the MSE of the conductivity parameters [ref. (21)] and the MSE of the activation time parameters [ref. (22)] of the whole tissue and the scar tissue areas around the conduction block, as highlighted in a red box in Fig. 7(c), (d), (h) and (i). Table 3 shows the parameter estimation errors of the whole tissue and the scar area obtained by the SCFA1 using one heart beat and the SCFA2 using five heart beats given uniform and non-uniform distributions of the electrodes. From Table 3 we find that for both types of tissue, SCFA2 achieves better estimation performance than SCFA1. The estimation of the parameters near the scar tissue is more challenging, as we can see that the estimation errors of the scar tissue are larger than the errors of the whole tissue. This can (partly) be explained by the fact that the scar tissue is relatively small compared to non-scar tissue and sampled by at most one or two electrodes. We also see that given a more random distribution of the sensor, the estimation

using the SCFA2 still performs better than SCFA1 and the conduction block areas are still detected. Since the underlying structure of tissue (ii) is more complicated than tissue (i), the estimation errors of tissue (ii) are larger than the errors of tissue (i). From Table 3, we also observe that the MSE difference of the conductivity estimation of the SCFA1 and the SCFA2 is about 0.01 near scar tissue given the non-uniform distribution of the electrodes, while the difference is about 0.07 given the uniform distribution of the electrodes. This implies that the estimation performance is related to the relative positions of the conduction block and the electrodes. Taking Tissue (i) as example, there are two electrodes exactly placed on top of the conduction block in the case of uniform placement of electrodes, which makes it easier to detect the block than the non-uniform placement of electrodes.

Fig. 8 shows examples of the real conductivity maps and the estimated conductivity maps of the 3D tissue. We observe that the estimation of the conductivity maps is further improved by the SCFA2 method using multiple heart beats compared to the SCFA1 method using a single heart beat.

5. Experiments on the clinical data

In this section, we evaluate the proposed method with clinical data.

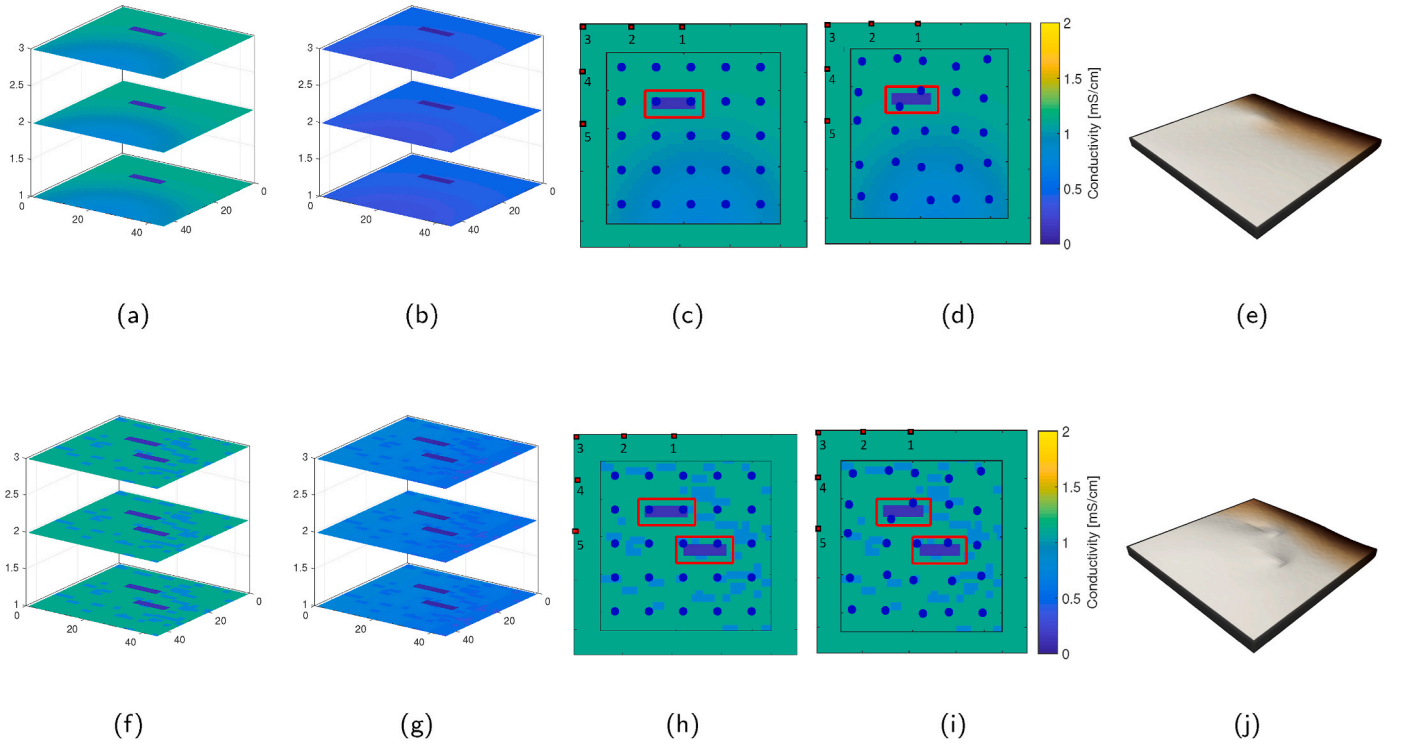


Fig. 7. Illustration of the 3D simulations. (a) and (b) Conductivity maps in the x-direction and the y-direction of tissue (i), respectively; (c) and (d) Uniform and non-uniform placement of the 25 electrodes on the top of tissue (i), respectively; (e) 3D plots of the action potential propagation in tissue (i) when $t = 200$ ms and when the stimuli are applied at position ‘1’ in (c); (f) and (g) Conductivity maps in the x-direction and the y-direction of tissue (ii), respectively; (h) and (i) Uniform and non-uniform placement of the 25 electrodes on the top of tissue (ii), respectively; (j) 3D plots of the action potential propagation in tissue (ii) when $t = 200$ ms and when the stimuli are applied at position ‘1’ in (h).

Table 3

Comparison of estimation errors with different methods for simulated 3D tissue.

Tissue Type	Tissue Area	Uniform Distribution				Non-Uniform Distribution			
		Err _c (SCFA1)	Err _c (SCFA2)	Err _a (SCFA1)	Err _a (SCFA2)	Err _c (SCFA1)	Err _c (SCFA2)	Err _a (SCFA1)	Err _a (SCFA2)
Tissue (i)	Whole Tissue	0.0377	0.0261	1.8204	1.8123	0.0311	0.0236	1.7614	1.7550
	Scar Tissue	0.2013	0.1328	7.2569	7.2146	0.1076	0.0945	6.5643	6.5411
Tissue (ii)	Whole Tissue	0.0603	0.0504	1.3754	1.3637	0.0516	0.0466	1.4123	1.4049
	Scar Tissue	0.2167	0.1449	3.6768	3.6510	0.1328	0.1227	3.9335	3.9349

These data are human atrial epicardial electrograms measured from patients during open heart surgery. The study protocol was approved in February 2010 by the Medical Ethics Committee (2010-054) in the Erasmus Medical Center, Rotterdam, The Netherlands. High resolution mapping arrays with 192 electrodes are used to measure the unipolar electrograms from different atrial epicardial sites. The distance between the neighboring electrodes is 2 mm. Five seconds of sinus rhythm and 10 s of atrial fibrillation are recorded at every mapping site and all recordings are sampled at 1 kHz. In this work we use recordings measured from Bachmann’s bundle during sinus rhythm. Readers can find more details on the mapping approach and the electrode array in [29]. The ventricular activities in the measurements are canceled by the method in [30] before doing the parameter estimation. The tissue is discretized into 192 equal square areas of $2\text{ mm} \times 2\text{ mm}$ and each area is assumed to have an electrode positioned on top of it. Each small area is then discretized into 3×3 cell groups and each cell group is regarded as a cell to reduce the number of unknowns for practical consideration. In each estimation, we take a smaller tissue area measured by 5×5 electrodes instead of the whole tissue area to reduce the computation cost, then the spatial resolution to be obtained is 15×15 , with resolution scale thus $R = 3$.

We consider that a cell can be activated only once in a time frame.

Before estimating the parameters, we first segmented the recording in heart beats and then one time frame includes one heart beat. The segment size is selected to include most of the information in one heart beat. Given the sampling rate of 1 kHz, each heart beat segment consists of 800 samples. Fig. 9 shows an example of the heart beat segmentation of an electrogram. We can see that the waveform shape varies among different heart beats, which motivates us to utilize different heart beats to increase the information for robust parameter estimation.

We used five consecutive heart beats from each recording and test the performance of the proposed algorithm when using one, two, three, four, and five heart beats, respectively. Since there is no ground truth of the real parameters, we evaluate the performance of the proposed method by comparing the real electrograms to the reconstructed electrograms obtained using the parameters estimated by the proposed method. Note that the conductivity parameters and the anisotropy ratio parameters are assumed to be similar for different heart beats while the activation time parameters differ across heart beats. We quantify the reconstruction errors of the electrograms by the reconstruction error

$$\text{Err}_{\text{rec}} = \frac{1}{M} \sum_{i=1}^M \|\mathbf{y}_m - \hat{\mathbf{y}}_m\|_2, \quad (23)$$

where \mathbf{y}_m and $\hat{\mathbf{y}}_m$ respectively represent the real and the estimated EGM

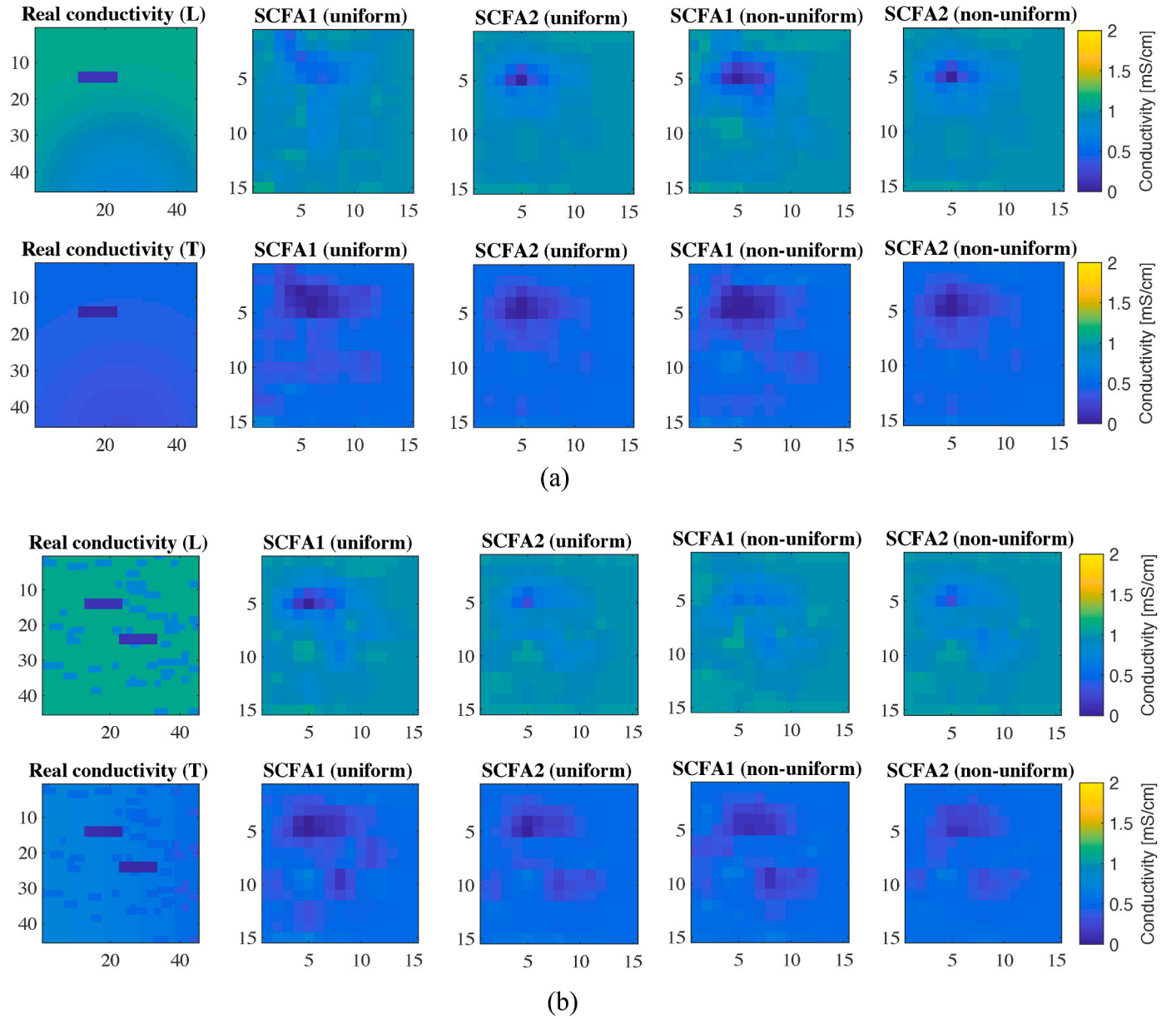


Fig. 8. Examples of the real conductivity maps and the estimated conductivity maps of the simulated 3D tissues. (a) Tissue type (i). (b) Tissue type (ii). The subfigures in the first column show the real conductivity maps in the Longitudinal (L) and transverse (T) directions. The subfigures in other columns show the estimated conductivity maps, which are obtained using different methods, including SCFA1 using one heart beat and SCFA2 using five heart beats given uniform electrode distribution and non-uniform electrode distribution.

segments during atrial activity, and $\|\cdot\|_2$ represents the l_2 -norm of a vector.

Fig. 10 shows the reconstruction errors of the electrograms from eight patients obtained by the proposed method when increasing the used number of heart beats from one to five. We see that in most cases the reconstruction error first decreases then tends to stabilize when increasing the number of heart beats for estimation, which demonstrates the added value of using multiple heart beats. For patient 1 and patient 3, the improvement obtained by increasing the number of heart beats for parameter estimation is small, which is possibly because the electrical waves in different heart beats of these patients have a very similar propagation pattern. We further compare the proposed method with the CMM method proposed in [10] and the SCFA1 method in [12]. Fig. 11 (a) shows the box plots of the reconstruction errors of the electrograms from eight patients using different methods. Overall, the reconstruction errors obtained by the SCFA2 method proposed in this work achieves

better performance, and SCFA1 performs on average slightly better than CMM in most of cases. Fig. 11(b) further shows the reconstruction errors of the electrograms of each patient. We see that the SCFA2 always achieves the best performance, as it combines the information of multiple heart beats. The obvious improvement obtained by SCFA2 can be found from Patient 3 to Patient 7, while the smaller improvements are obtained from Patient 1, Patient 2, and Patient 8. This is possibly because the heart beats are similar in these patients and adding additional heart beats does not give much additional information for parameter estimation in SCFA2. For Patient 1, Patient 2, and Patient 8, the performance of the three methods are close, although SCFA1 and SCFA2 consider more realistic conditions and use less assumption to simplify the problem compared to CMM. This might be because the number of unknown parameters with SCFA1 and SCFA2 is larger than with CMM. This means it is more challenging to find the optimal solution when solving the non-convex optimization problem.

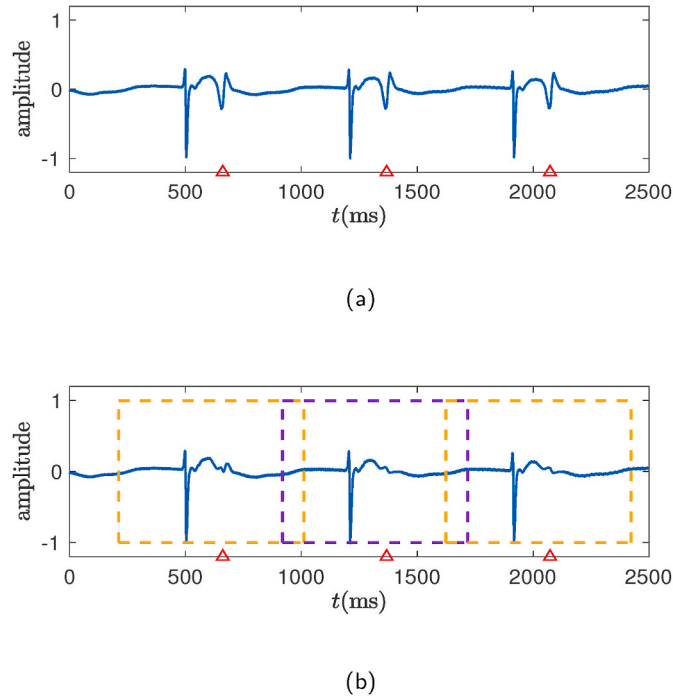


Fig. 9. Epicardial electrogram examples before (a) and after (b) canceling ventricular activity and heart beat segmentation example. The red triangle marks the presence of ventricular activity. The orange and purple boxes mark the heart beat segments.

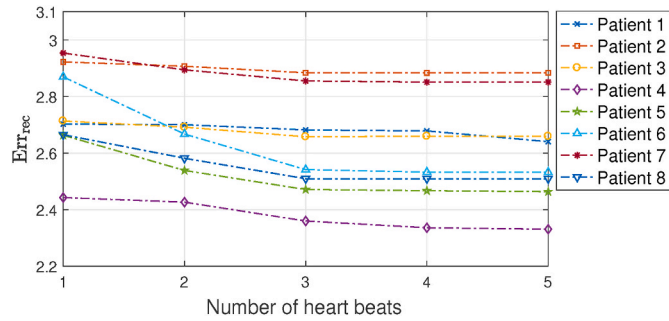


Fig. 10. Reconstruction errors of electrograms from eight patients using different number of heart beats for parameter estimation.

The plots in Figs. 12 and 13 give two examples of the estimated activation time maps, the conductivity maps, and the real and the reconstructed electrograms of two patients obtained using five heart beat segments for parameter estimation. Figs. 12 (a) and 13 (a) show the estimated activation time maps obtained by the steepest descent method and Fig. 12 (b) and 13 (b) show the estimated activation time maps obtained by the proposed method, from which we can see some differences between the estimated activation time obtained by the two methods. Subfigures (c) and (d) in Figs. 12 and 13 show estimated conductivity maps in the longitudinal direction and the transverse direction obtained by the SCFA2 method, respectively. Figs. 12 (e) and 13 (e) show examples of the real epicardial electrograms and the reconstructed epicardial electrograms obtained with the parameters estimated by the proposed method using different number of heart beats, respectively. From Figs. 12 (e) and Fig. 13 (e) we observe that in most cases the reconstructed electrograms match better the real electrograms when increasing the number of heart beats. As shown in Fig. 12 (e), the electrogram segments with a single deflection can be reconstructed quite well. From the EGM examples measured at the electrode positions ‘E3’

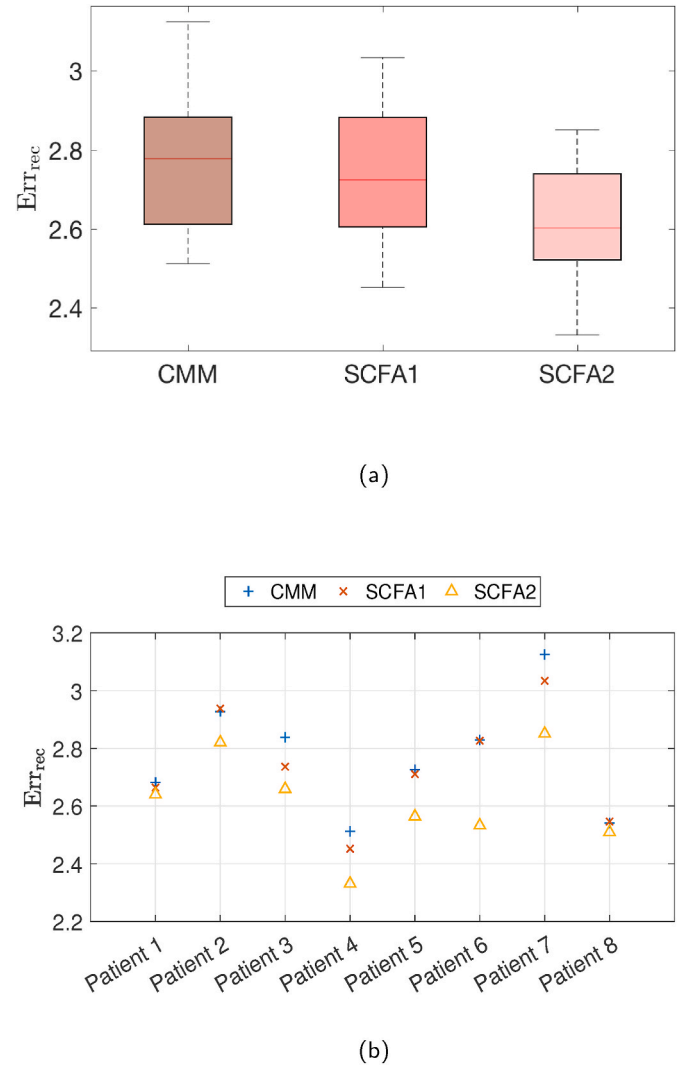


Fig. 11. Reconstruction errors of the electrograms from eight patients using CMM, SCFA1, and SCFA2 for parameter estimation. (a) Box plots of the reconstruction errors of the eight patients. (b) The reconstruction error of the electrograms for each patient.

and ‘E4’ in Fig. 13 (e), we see that using multiple heart beats helps to reconstruct the electrograms having double potentials. However, at the electrode position ‘E1’ in 13 (e), increasing the number of heart beat does not obviously improve the reconstruction. This may be, because the EGM segments of different heart beats are too similar.

6. Computational complexity analysis

The optimization of the proposed method is computational complex due to the large number of unknown parameters. According to the two identifiability conditions in Section 3.2, the total number of knowns due to $\hat{\Phi}_y(k, l)$ for $\forall k \in S_f, \forall l \in S_l$ is $|S_l||S_f|M^2$ and the total number of unknowns due to $\sigma, \alpha, \tau_n, n = 1, \dots, N-1$ for $\forall l \in S_b$ and $\hat{\Phi}_u(k, l)$ for $\forall k \in S_f, \forall l \in S_l$ to be estimated is $n = 2N + |S_l|(N-1) + |S_f||S_l|M$. The optimization problem includes four inequality constraints on the power spectral density of the sensor self noise, i.e., $q_m(k, l) \geq 0, m = 1, 2, \dots, M$ for $\forall k \in S_f, \forall l \in S_b$, on the anisotropy ratio, i.e., $0 \leq \alpha \leq \alpha_{upper}$, on the conductivity, i.e., $0 \leq \sigma \leq \sigma_{upper}$, and on the activation time of the cells except the reference cell, i.e., $\tau_{low} \leq \tau_n(l) \leq \tau_{upper}, n = 1, \dots, N-1$ for $\forall l \in S_b$ and two linear equality constraints on the activation time of the reference cell, i.e., $\tau_0(l) = 0$ for $\forall l \in S_l$ and on the power spectral density

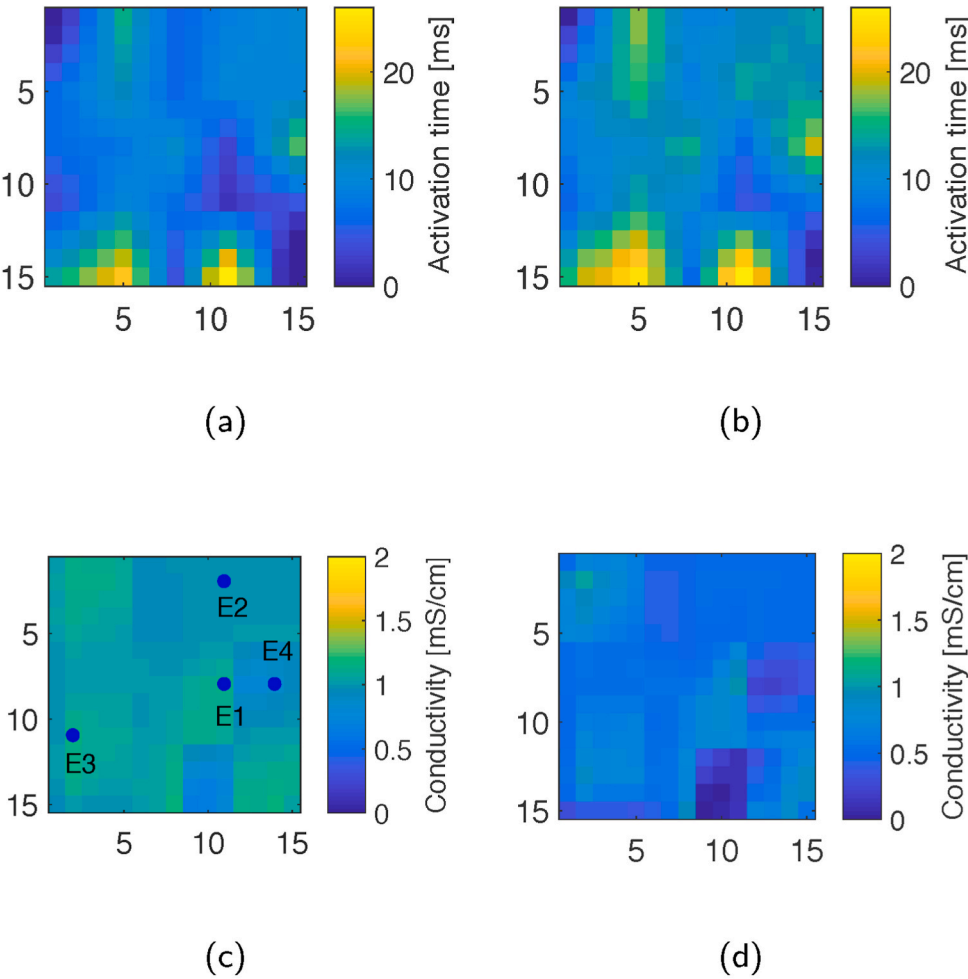
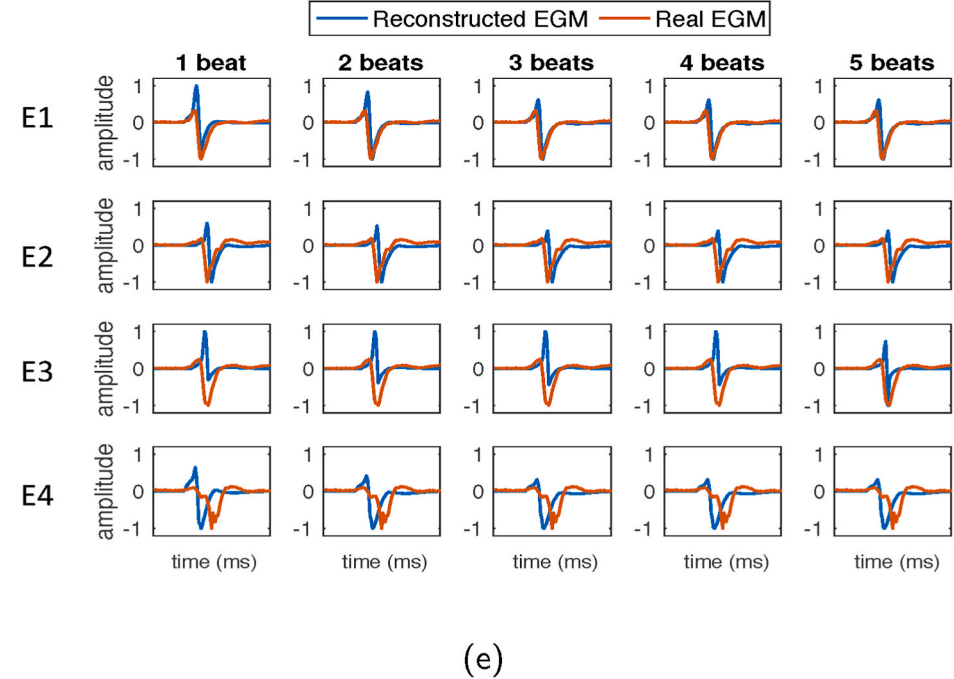


Fig. 12. Example of estimated conductivity maps, the real epicardial electrogram (EGM) and the reconstructed EGM obtained with the parameters estimated by the proposed method using different number of heart beats of patient 5. (a) and (b) show the estimated activation time maps for obtained by the steepest descent method and the SCFA2 method, respectively. (c) and (d) show estimated conductivity maps in the longitudinal direction and the transverse direction obtained by the SCFA2 method, respectively. (e) shows the real EGMs (red) and the reconstructed EGMs (blue) measured at the electrode positions (marked by the blue points) in (c), respectively.



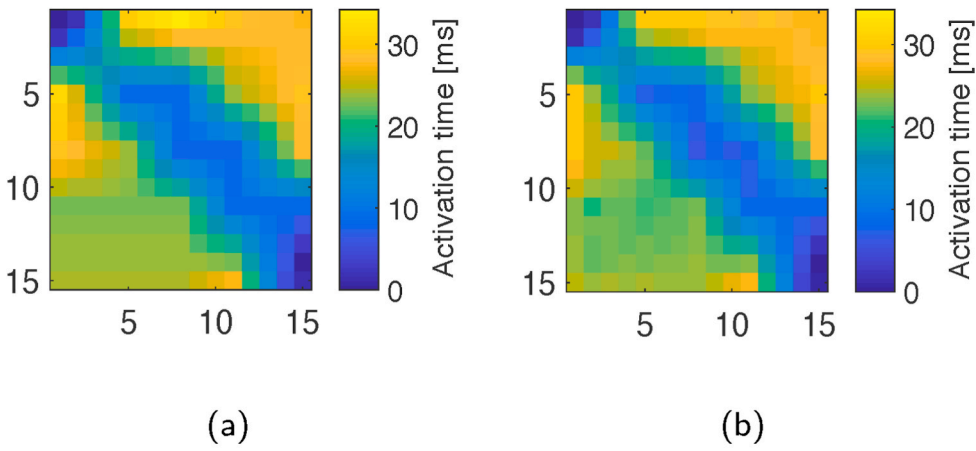
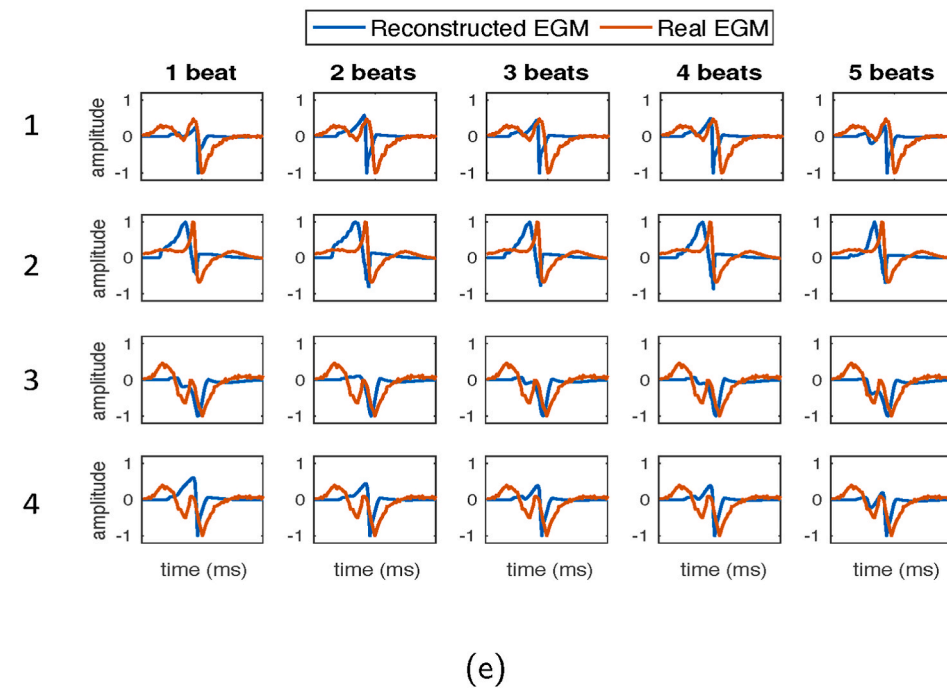
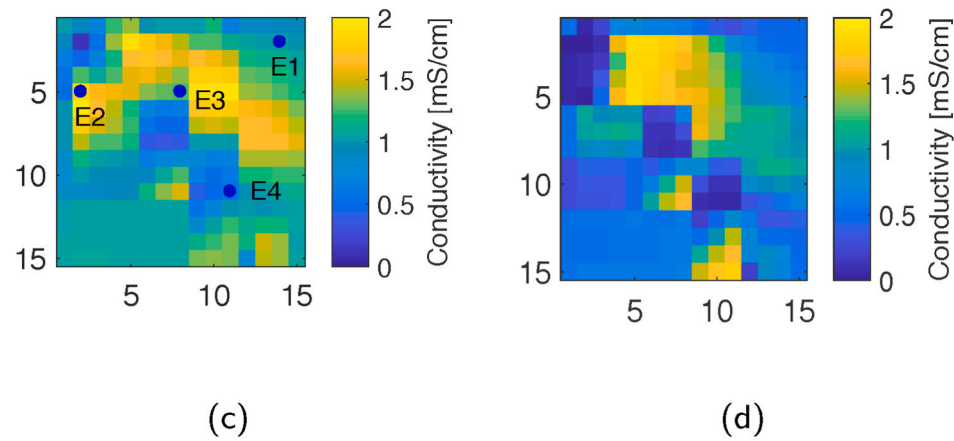


Fig. 13. Example of estimated conductivity maps, the real epicardial electrogram (EGM) and the reconstructed EGM obtained with the parameters estimated by the proposed method using different number of heart beats of patient 6. (a) and (b) show the estimated activation time maps obtained by the steepest descent method and the SCFA2 method, respectively. (c) and (d) show estimated conductivity maps in the longitudinal direction and the transverse direction obtained by the SCFA2 method, respectively. (e) shows the real EGMs (red) and the reconstructed EGMs (blue) measured at the electrode positions (marked by the blue points) in (c), respectively.



of the reference cell, i.e., $\varphi(k, l) = \tilde{\varphi}(k, l)$ for $\forall k \in S_f, \forall l \in S_l$. The optimization problem is computational complex and solved by the ‘fmincon Interior Point Algorithm’ using the optimization toolbox in Matlab. The first reasonably efficient Interior Point algorithm was proposed by Karmark in 1984 and the overall complexity of this algorithm is $O(n^{3.5}L^2)$, with n the number of variables and L the binary encoding length of the input data [31]. Usually the constraints can lead to a speed up in the solution process. Therefore the upper bound of the complexity of the optimization problem would be $O(n^{3.5}L^2)$.

To give an idea of the complexity, we also provide the computational time of different algorithms for comparison. The algorithms are implemented using MATLAB on an office laptop with 2.9 GHz Intel Core i5 processor and 8 GB RAM memory. Table 4 shows the computational time for different methods averaged per heart beat. Note that different methods have been proposed to estimate different parameters. Compared to the reference methods, the SCFA2 method proposed in this work estimates much more parameters and therefore its computational time is higher. However, the proposed method also clearly leads to improvements. This implies future work is needed to further lower the complexity of the proposed method while still having the same performance.

7. Conclusions and discussions

In this work, we proposed a novel algorithm to jointly estimate tissue properties using the cross power spectrum model of microelectrode array data in combination with confirmatory factor analysis (CFA). Based on the reasonable assumption that the conductivity and anisotropy ratio parameters are similar among multiple heart beats and frequencies, we proposed to estimate these parameters using multiple heart beats and frequencies with the simultaneous CFA (SCFA). The activation time of cells are also estimated jointly with these parameters but will be different across heart beats. With the SCFA algorithm, we are able to determine the resolution that can be obtained with a given amount of data. Compared to the previously published SCFA for conductivity estimation in [12], the proposed SCFA in this work makes use of multiple heart beats which “illuminate” the tissue from different directions and can therefore better estimate the tissue properties. Experiments on simulated data and clinical data demonstrate that the proposed SCFA method obtains good estimation of the tissue conductivity and reconstructs realistic electrograms that match the clinical data well.

This work provides an efficient tool to estimate the hidden parameters of diseased tissue, which is helpful in the understanding and diagnosis of the disease. Intended applications of this work can be automated detection of the atrial areas of bad conduction and finding the relation between the alternations of atrial conduction and the initiation and perpetuation of cardiac arrhythmias in order to guide therapy methods like cardiac ablation.

Although conduction velocity, which looks at the propagation of the action potential, has been commonly used to determine the areas of conduction block, the findings are realization dependent, since the abnormalities are determined based on the output realizations of the system, i.e., on the wave propagation. Moreover, looking at (pairs of) electrodes, not all spatial correlations between the different measurements are taken into account. This is unlike the proposed method, which considers the heart as the system, where each cell or area of cells has certain properties that are important to understand the arrhythmias like atrial fibrillation. With the proposed method, we can determine the parameters that describe the underlying system, such as the conductivity, anisotropy ratio, etc. Knowing the system (or its parameters) that can generate the realizations that we measure as electrograms is the ultimate goal.

Although the proposed method has its advantages on jointly estimating the parameters of cardiac tissue, it still needs to be improved by taking into account more realistic electrophysiological conditions in real tissue. For example, the assumption of a common stereotypic action

Table 4

Computational time of different methods.

Methods	Estimated parameters	Number of estimated parameters	Run time per heart beat	Estimation error of conductivity
CV	cv	1	0.1 s	–
CMM	σ	225 due to σ	158.3 s	0.0455
SCFA1	σ, α, Φ_u	225 due to σ 225 due to α 2500 due to Φ_u	2148.5 s	0.0418
SCFA2	$\sigma, \alpha, \Phi_u, \tau_n(n = 1, \dots, N - 1)$	225 due to σ 225 due to α 2500 \times 4 due to Φ_u 224 \times 4 due to τ_n	3357.0 s	0.0295

1. Notation: cv : conduction velocity; σ : conductivity; α : anisotropy ratio; Φ_u : noise PSDM; $\tau_n(n = 1, \dots, N - 1)$: activation time.

2. The desired spatial resolution for the estimation is $15 \times 15 = 225$, the number of electrodes M is 25, and the number of frequency bands $|S_f|$ is 100.

3. In this comparison, four heart beats are used for parameter estimation.

potential waveform for all cells reduces the computational cost for estimation, but ignores the heterogeneities in atrial tissue and reduces the accuracy of the model. The assumption that conductivity tensors are aligned along the axes ignores the heterogeneous tissue micro-structure and the two-dimensional assumption of tissue makes the application limited to only thin-walled tissues. Although the proposed method works well for the SR data, for more complicated situations in a large dataset, the model needs to be further improved. In the near future, we would like to take into account more realistic conditions, such as multi-layers of tissue, orientation of the fibers, etc, to improve the model. To do so, there are more parameters needed to describe the structure of the tissue, which will in turn increase the computational complexity of estimating the model parameters. However, a critical issue in this area is reducing complexity of the model to make it possible to solve complicated inverse problems for tissue parameter estimation. Therefore, we will take into account both the accuracy of the model and the computational complexity of parameter estimation in future work. Since there are various ways to construct the discrete models of tissue geometry, we would also like to investigate the impact of the discrete representations of tissue geometry on the parameter estimation. The standard spatial models of tissue geometry include both 2D and 3D tissue segments. It is common to construct a regular mesh with uniform elements to approximate the tissue surface, such as the square lattice that we used in this work, or an irregular mesh with uniform elements. Although irregular meshes can improve the representation of a curved surface, such mesh generation is more difficult and the numerical methods associated with irregular meshes require a higher computational cost, as discussed in [6]. It still remains challenge to construct meshes that accurately represent the complicated 3D tissue geometry, although mesh generation tools have been developed in other engineering fields [6]. It is also an interesting topic we would like to explore in the future work.

Author contributions

All authors have participated sufficiently in this work. M. Sun designed the algorithm, performed the experiments, and was the main writer of the manuscript. N. M.S. de Groot provided the clinical dataset, provided suggestions on the clinical aspects, and provided the clinical interpretation of the model. R. C. Hendriks designed the algorithm, guided the experiments, and co-wrote the manuscript. All authors reviewed the manuscript.

Declaration of competing interest

None Declared.

References

- [1] C.D. Cantwell, C.H. Roney, F.S. Ng, J.H. Siggers, S.J. Sherwin, N.S. Peters, Techniques for automated local activation time annotation and conduction velocity estimation in cardiac mapping, *Comput. Biol. Med.* 65 (2015) 229–242.
- [2] M.S. van Schie, A. Heida, Y.J.H.J. Taverne, A.J.J.C. Bogers, N.M.S. de Groot, Identification of local atrial conduction heterogeneities using high-density conduction velocity estimation, *Europace* (2021), euab088.
- [3] N. Mazeh, D.E. Haines, M.W. Kay, B.J. Roth, A simplified approach for simultaneous measurements of wavefront velocity and curvature in the heart using activation times, *Cardiovasc. Eng. Technol.* 4 (4) (2013) 520–534.
- [4] A.G. Kléber, Y. Rudy, Basic mechanisms of cardiac impulse propagation and associated arrhythmias, *Physiol. Rev.* 84 (2) (2004) 431–488.
- [5] F.M. Weber, A. Luik, C. Schilling, G. Seemann, M.W. Krueger, C. Lorenz, C. Schmitt, O. Dossel, Conduction velocity restitution of the human atrium? an efficient measurement protocol for clinical electrophysiological studies, *IEEE (Inst. Electr. Electron. Eng.) Trans. Biomed. Eng.* 58 (9) (2011) 2648–2655.
- [6] R.H. Clayton, et al., Models of cardiac tissue electrophysiology: progress, challenges and open questions, *Prog. Biophys. Mol. Biol.* 104 (2010).
- [7] C.S. Henriquez, A brief history of tissue models for cardiac electrophysiology, *IEEE (Inst. Electr. Electron. Eng.) Trans. Biomed. Eng.* 61 (5) (2014) 1457.
- [8] R. Plonsey, R.C. Barr, *Bioelectricity: a Quantitative Approach*, Springer Science & Business Media, 2007.
- [9] E. Gilboa, P.S. La Rosa, A. Nehorai, Estimating electrical conductivity tensors of biological tissues using microelectrode arrays, *Ann. Biomed. Eng.* 40 (10) (2012) 2140–2155.
- [10] B. Abdi, R.C. Hendriks, A.-J. van der Veen, N.M. de Groot, A compact matrix model for atrial electrograms for tissue conductivity estimation, *Comput. Biol. Med.* 107 (2019) 284–291.
- [11] G. Salama, et al., Subthreshold simulation of purkinje fibers interrupts ventricular tachycardia in intact hearts, *Circ. Res.* 74 (4) (1994) 604–619.
- [12] M. Sun, N.M.S. de Groot, R.C. Hendriks, Cardiac tissue conductivity estimation using confirmatory factor analysis, *Comput. Biol. Med.* 135 (2021).
- [13] T.A. Brown, M.T. Moore, *Confirmatory Factor Analysis, Handbook of Structural Equation Modeling*, 2012, pp. 361–379.
- [14] D.N. Lawley, A.E. Maxwell, Factor analysis as a statistical method, *J. Roy. Stat. Soc. Series D (The Statistician)* 12 (3) (1962) 209–229.
- [15] K.G. Jöreskog, A general approach to confirmatory maximum likelihood factor analysis, *Psychometrika* 34 (2) (1969) 183–202.
- [16] K.G. Jöreskog, D.N. Lawley, New methods in maximum likelihood factor analysis, *Br. J. Math. Stat. Psychol.* 21 (1) (1968) 85–96.
- [17] A.I. Koutrouvelis, R.C. Hendriks, R. Heusdens, J. Jensen, Robust joint estimation of multimicrophone signal model parameters, in: *IEEE/ACM Transactions on Audio, Speech, and Language Processing* 27, 2019, pp. 1136–1150, 7.
- [18] C. Gabriel, S. Gabriel, E. Corthout, The dielectric properties of biological tissues: I. literature survey, *Phys. Med. Biol.* 41 (11) (1996) 2231.
- [19] C.D. Cantwell, C.H. Roney, F.S. Ng, J.H. Siggers, S.J. Sherwin, N.S. Peters, Techniques for automated local activation time annotation and conduction velocity estimation in cardiac mapping, *Comput. Biol. Med.* 65 (2015) 229–242.
- [20] M. Potse, et al., A comparison of monodomain and bidomain reaction-diffusion models for action potential propagation in the human heart, *IEEE Trans. Biomed. Eng.* 53 (12) (2006) 2425–2435.
- [21] B.F. Nielsen, et al., Optimal monodomain approximations of the bidomain equations, *Appl. Math. Comput.* 184 (2007) 276–290.
- [22] Y. Coudière, Y. Bourgault, M. Rioux, Optimal monodomain approximations of the bidomain equations used in cardiac electrophysiology, *Math. Model Methods Appl. Sci.* 24 (2014) 1115–1140.
- [23] N. Virag, V. Jacquemet, C. Henriquez, S. Zozor, O. Blanc, J.-M. Vesin, E. Pruvot, L. Kappenberger, Study of atrial arrhythmias in a computer model based on magnetic resonance images of human atria, *Chaos: Interdiscipl. J. Nonlinear Sci.* 12 (3) (2002) 754–763.
- [24] R.H. Byrd, M.E. Hribar, J. Nocedal, An interior point algorithm for large scale nonlinear programming, *SIAM J. Optim.* 9 (4) (1999).
- [25] R.H. Byrd, J.C. Gilbert, J. Nocedal, A trust region method based on interior point techniques for nonlinear programming, *Math. Program.* 89 (1) (2000) 149–185.
- [26] R.A. Waltz, J. Morales, J. Nocedal, D. Orban, An interior algorithm for nonlinear optimization that combines line search and trust region steps, *Math. Program.* 107 (3) (2006) 391–408.
- [27] M.R. Courtemanche, R.J. Ramirez, S. Nattel, Ionic mechanisms underlying human atrial action potential properties: insights from a mathematical model, *Am. J. Physiol. Heart Circ. Physiol.* 275 (1) (1998) H301–H321.
- [28] J. Solomon, *Numerical Algorithms: Methods for Computer Vision, Machine Learning, and Graphics*, CRC press, 2015.
- [29] A. Yaksh, L.J. van der Does, C. Kik, P. Knops, F.B. Oei, P.C. van de Woestijne, J. A. Bekkers, A.J. Bogers, M.A. Allesie, N.M. de Groot, A novel intra-operative, high-resolution atrial mapping approach, *J. Intervent. Card Electrophysiol.* 44 (3) (2015) 221–225.
- [30] M. Sun, E. Isufi, N.M.S. de Groot, R.C. Hendriks, Graph-time spectral analysis for atrial fibrillation, *Biomed. Signal Process Control* 59 (2020).
- [31] N. Karmarkar, A new polynomial-time algorithm for linear programming, in: *Proceedings of the Sixteenth Annual ACM Symposium on Theory of Computing*, 1984, pp. 302–311.